Stem Cell Reports
Article

ISSCR

OPEN ACCESS

2i Maintains a Naive Ground State in ESCs through Two Distinct Epigenetic Mechanisms

Ye-Ji Sim,[1,5] Min-Seong Kim,[1,5] Abeer Nayfeh,[1,5] Ye-Jin Yun,[1] Su-Jin Kim,[1] Kyung-Tae Park,[2] Chang-Hoon Kim,[3,*] and Kye-Seong Kim[1,4,*]

[1]Department of Biomedical Science, Graduate School of Biomedical Science and Engineering, Hanyang University, Seoul 04763, Republic of Korea
[2]Department of Pathology and Laboratory Medicine, Center for Cancer Research, University of Tennessee Health Science Center, Memphis, TN 38103, USA
[3]Department of Pharmacology, Korea University College of Medicine, Seoul 02841, Republic of Korea
[4]Department of Anatomy and Cell Biology, College of Medicine, Hanyang University, Seoul 04763, Republic of Korea
[5]Co-first author
*Correspondence: chakimster@korea.ac.kr (C.-H.K.), ks66kim@hanyang.ac.kr (K.-S.K.)
http://dx.doi.org/10.1016/j.stemcr.2017.04.001

SUMMARY

Mouse embryonic stem cells (ESCs) are maintained in serum with leukemia inhibitory factor (LIF) to maintain self-renewal and pluripotency. Recently, a 2i culture method was reported using a combination of MEK inhibition (MEKi) and GSK3 inhibition (GSK3i) with LIF to maintain ESCs in a naive ground state. How 2i maintains a ground state of ESCs remains elusive. Here we show that MEKi and GSK3i maintain the ESC ground state by downregulating global DNA methylation through two distinct mechanisms. MEK1 phosphorylates JMJD2C for ubiquitin-mediated protein degradation. Therefore, MEKi increased JMJD2C protein levels but decreased DNMT3 expression. JMJD2C promotes TET1 activity to increase 5-hydroxymethylcytosine (5hmC) levels. GSK3i suppressed DNMT3 expression, thereby decreasing DNA methylation without affecting 5hmC levels. Furthermore, 2i increased PRDM14 expression to inhibit DNMT3A/B protein expression by promoting G9a-mediated DNMT3A/B protein degradation. Collectively, 2i allows ESCs to maintain a naive ground state through JMJD2C-dependent TET1 activation and PRDM14/G9a-mediated DNMT3A/B protein degradation.

INTRODUCTION

Early mouse zygotes differentiate in the trophectoderm and inner cell mass (ICM). Mouse embryonic stem cells (ESCs) are derived from the ICM in mouse embryos (Evans and Kaufman, 1981; Martin, 1981). ESCs are usually maintained in serum supplemented with leukemia inhibitory factor (LIF), which keeps them in a pluripotent state capable of self-renewal (Smith et al., 1988; Williams et al., 1988) through the activation of JAK-STAT3 signaling (Matsuda et al., 1999; Niwa et al., 1998). Serum/LIF generates a heterogeneous population of ESCs by causing auto-inductive stimulation of the MAPK/ERK pathway by fibroblast growth factor (FGF) 4 (Kunath et al., 2007; Stavridis et al., 2007; Ying et al., 2008). Ying et al. (2008) proposed that LIF and bone morphogenetic protein signals act downstream of the ERK pathway to block ESC commitment. To maintain a ground state in ESCs, they used three selective small-molecule inhibitors, SU5402, PD0325901, and CHIR99021, to inhibit FGF receptor (FGFR) tyrosine kinases, the ERK pathway, and Wnt signaling, respectively (Ying et al., 2008). Later, the use of two inhibitors, PD0325901 and CHIR99021 (called 2i), with LIF to block the MAPK/ERK and glycogen synthase kinase 3β (GSK3β) pathways was postulated to be sufficient to maintain the ESC ground state (Silva et al., 2008). ESCs cultivated in a serum-free 2i medium with LIF (2i ESCs) exhibit greater pluripotent gene expression than ESCs cultivated in serum with LIF (serum ESCs). Further, 2i ESCs homogeneously express NANOG, which potentiates pluripotent gene transcription by creating a permissive chromatin structure (Marks et al., 2012; Marks and Stunnenberg, 2014; Miyanari and Torres-Padilla, 2012; Silva et al., 2009). In addition, 2i leads to genome-wide DNA hypomethylation due to reduced expression of the DNA methyltransferase 3 (DNMT3) family (Bagci and Fisher, 2013; Leitch et al., 2013). The mechanism by which 2i creates a permissive chromatin structure and downregulates DNMT3 expression remains undefined.

DNA methylation by the DNMT family is a heritable epigenetic modification involved in gene silencing, imprinting, and retrotransposon suppression (Baylin, 2005; Jin et al., 2011). In mammals, there are four major members of the DNMT family: DNMT1, DNMT3A, DNMT3B, and DNMT3L. DNMT3A and DNMT3B share similar domain structures: an N-terminal variable region, followed by a PWWP domain, a cysteine-rich zinc-binding domain, and a C-terminal catalytic domain. DNMT3L has no catalytic activity by itself because it lacks the C-terminal catalytic domain (Subramaniam et al., 2014). The DNMT family is dynamically regulated during mouse development (Smith et al., 2012). Global DNA hypomethylation by *Dnmt1*$^{-/-}$ and *Dnmt3a*$^{-/-}$,*3b*$^{-/-}$ in ESCs blocks differentiation and induces histone hyperacetylation (Lei et al., 1996; Okano et al., 1999).

In ESCs, G9a, a nuclear histone lysine methyltransferase (HMT) that methylates histones H1, H3K9, and H3K27 (Tachibana et al., 2001; Wu et al., 2011), recruits DNMT3A/B

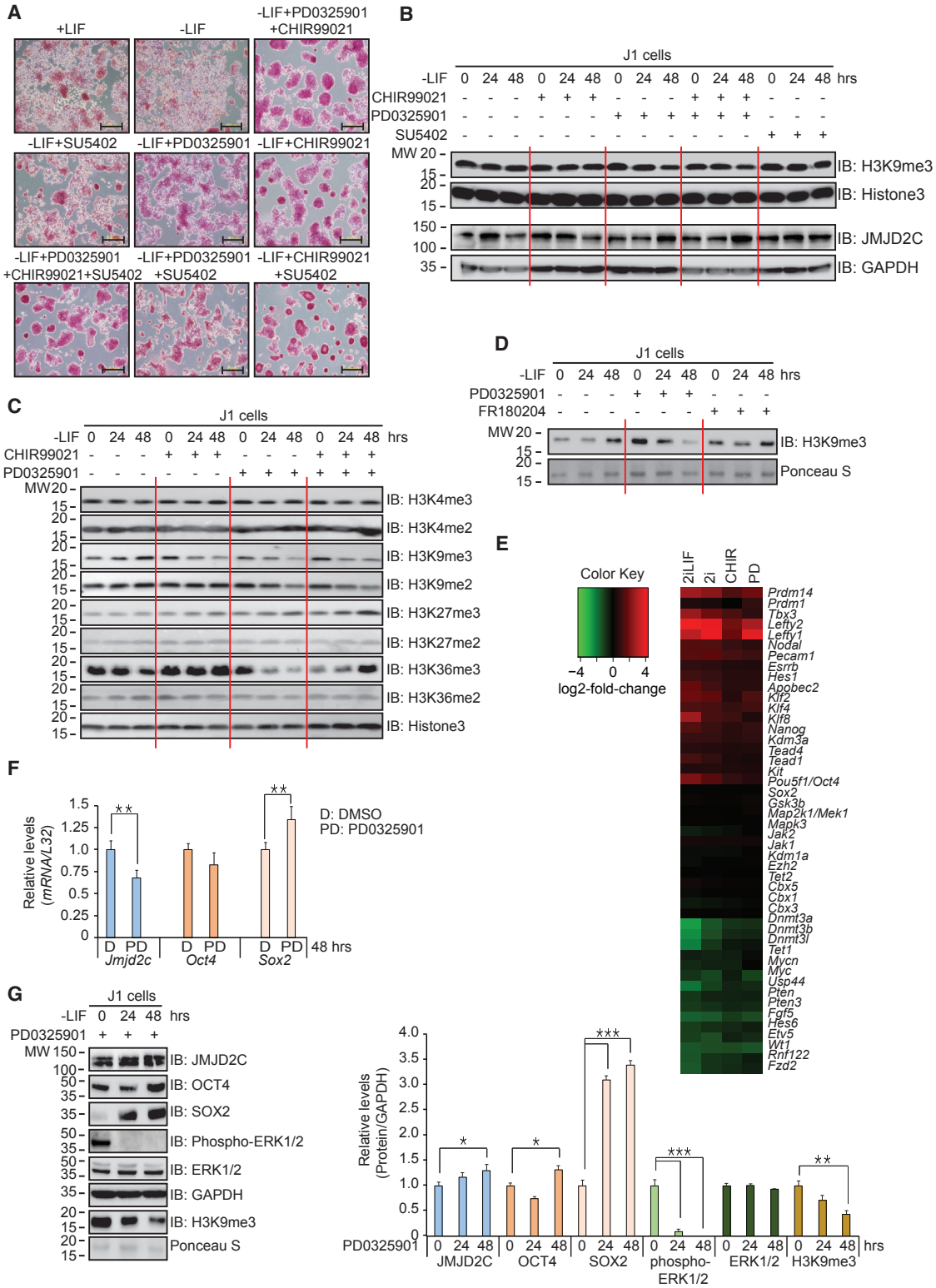

Figure 1. MEK Inhibition Regulates JMJD2C Stabilization and Decreases H3K9me3 Levels

(A) AP staining shows that combinatorial treatments of three small-molecule inhibitors induce pluripotency in ESCs. Scale bar, 200 μm.

(B) Western blots show that PD0325901 increases JMJD2C protein levels and decreases H3K9me3 levels. ESCs were cultured in feeder-free and LIF-free conditions with inhibitors for 24 and 48 hr.

(legend continued on next page)

independently of its HMT activity (Epsztejn-Litman et al., 2008). G9a contains a SET domain with ankyrin repeats and mediates the transfer of one to three methyl groups from S-adenosylmethionine to the amino group of a target lysine (Esteve et al., 2005), resulting in gene silencing (Dillon et al., 2005; Tachibana et al., 2001). G9a also methylates non-histone proteins, such as p53, WIZ, CDYL1, ACINUS, REPTIN, MYOD, and DNMT1, to regulate chromatin structure and transcriptional machinery (Jung et al., 2015; Ling et al., 2012; Rathert et al., 2008). The mechanism underlying G9a-mediated DNMT3A/B regulation in ESCs is not well understood.

JmjC domain-containing histone demethylase 2C (JMJD2C) is a histone lysine demethylase (HDM) specific for histones H3K9me3, H3K9me2, and H3K36me3 (Cloos et al., 2006; Klose et al., 2006; Whetstine et al., 2006). HDMs are histone-modifying enzymes with biological functions opposite to those of HMTs. JMJD2C removes the repressive histone-methylation at the promoters of pluripotent genes in ESCs. The JMJD2C-mediated reduction of H3K9me3 levels and the resulting alteration of chromatin structure are essential for maintaining ESC pluripotency (Das et al., 2014; Loh et al., 2007; Pedersen et al., 2014). Recent studies demonstrated that JMJD2B and JMJD2C are necessary for ESC self-renewal and induce the generation of pluripotent stem cells (Das et al., 2014; Pedersen et al., 2014). Therefore, JMJD2C acts to maintain ESC self-renewal and pluripotency by lowering H3K9me3 levels (Chen et al., 2013a; Loh et al., 2007; Ng and Surani, 2011).

PR/SET domain 14 (PRDM14) plays a role in the maintenance of the core pluripotent circuitry in ESCs by reducing protein levels of the DNMT3 family (Grabole et al., 2013; Hackett et al., 2013a; Yamaji et al., 2013). PRDM14 is a key regulator in the specification of primordial germ cells (PGCs) during mouse development (Yamaji et al., 2008). PRDM14 is a PR domain-containing (PRDM) transcription factor that contains a PR domain, a modified SET domain, and six tandemly repeated zinc fingers (Nakaki and Saitou, 2014). Downregulation of the DNMT3 family by PRDM14 is important for establishing genome-wide DNA hypomethylation in 2i culture conditions (Grabole et al., 2013; Hackett et al., 2013a; Yamaji et al., 2013). The mechanism by which PRDM14 regulates DNMT3 expression remains undefined.

The ten-eleven translocation (TET) family of dioxygenases promotes DNA demethylation in ESCs and PGCs (Ito et al., 2010; Koh et al., 2011; Vincent et al., 2013). The TET family converts 5-methylcytosine (5mC) to 5-hydroxymethylcytosine (5hmC), 5-formylcytosine, and 5-carboxylcytosine through a series of active DNA demethylation reactions (Gu et al., 2011; Hackett et al., 2013b; Tahiliani et al., 2009). Therefore, the TET family reduces genome-wide DNA methylation through the production of unmethylated cytosine aided by thymine-DNA glycosylase (Kohli and Zhang, 2013; Shen et al., 2013). In ESCs, TET1 is highly expressed and is required for self-renewal (Ito et al., 2010). The mechanism by which 2i treatment enhances TET1 activity is not yet known.

The purpose of this study was to elucidate two distinct epigenetic mechanisms by which 2i maintains the naive ground state in ESCs. 2i upregulated DNA hydroxymethylation by JMJD2C-mediated TET1 potentiation and decreased genome-wide DNA methylation through PRDM14/G9a-dependent DNMT3A/B protein degradation.

RESULTS

MEK Inhibition Stabilizes JMJD2C Proteins and Decreases H3K9me3 Levels

Murine ESCs have been maintained in serum with LIF to maintain their self-renewal (Smith et al., 1988; Williams et al., 1988). However, Ying et al. (2008) reported that a culture method maintained a ground state in ESCs. This medium was supplemented with three small-molecule inhibitors, PD0325901, CHIR99021, and SU5042, which inhibit MAPK/ERK, GSK3β, and FGFR signaling, respectively. Subsequently, they showed that 2i, PD0325901, and CHIR99021, with LIF (2i/LIF condition) is sufficient to sustain a ground state in ESCs (Silva et al., 2008). Therefore, we have examined how each of the three inhibitors influence the maintenance of a naive state in ESCs.

LIF treatment affects JAK-STAT as well as MAPK/ERK signaling for the maintenance of ESC self-renewal (Cherepkova et al., 2016; Onishi and Zandstra, 2015). In agreement with that, we found that LIF increased alkaline phosphatase (AP) activity, which is indicative of increased stemness (Figure 1A). Therefore, we limited the addition of LIF in our

(C) PD0325901 and/or CHIR99021 induce changes of histone H3 methylation in feeder-free and LIF-free ESCs.
(D) MEKi with PD0325901 decreases H3K9me3 levels in ESCs, but not ERKi with FR180204 in western blots.
(E) Combinatorial 2i treatments change gene expression in ESCs. Data come from the GEO DataSet (GEO: GSE43597). The 2i treatments upregulate *Prdm14* and downregulate the *Dnmt3* family.
(F) qRT-PCR (n = 4 independent experiments) shows that PD0325901 decreases *Jmjd2c* mRNA levels compared with the DMSO control.
(G) Western blots show that PD0325901 increases JMJD2C, OCT4, and SOX2 protein levels but decreases H3K9me3 levels (n = 3 independent experiments).
*p < 0.05, **p < 0.01, ***p < 0.001.

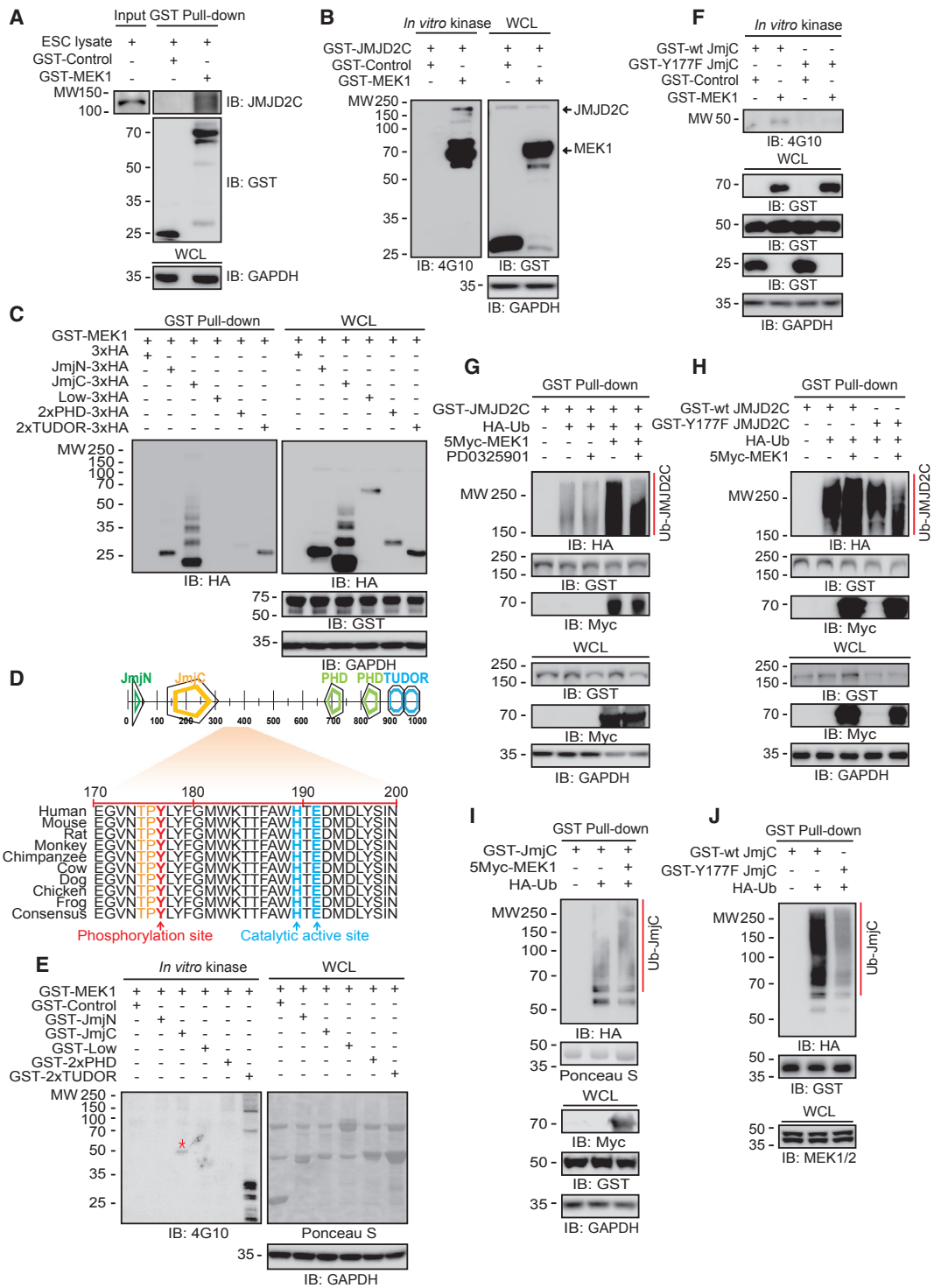

Figure 2. MEK1 Interacts with and Phosphorylates JMJD2C, Which Undergoes Phosphorylation-Dependent Degradation through the Ubiquitin-Pproteasome Pathway

(A) GST pull-down assay shows that MEK1 associates with endogenous JMJD2C.

(B) An in vitro MEK1 kinase assay performed with mouse anti-phosphotyrosine-specific 4G10 antibody shows that MEK1 phosphorylates tyrosine residues of JMJD2C.

(C) MEK1 binds to the JmjN, JmjC, 2×PHD, and 2×TUDOR domains in JMJD2C.

(legend continued on next page)

experimental conditions to discriminate between LIF-mediated effects and inhibitor-mediated effects. In the absence of LIF, MEK inhibition (MEKi) by PD0325901 produced intense AP staining with compact ESC morphology. GSK3 inhibition (GSK3i) by CHIR99021 resulted in strong AP staining characterized by a dome-shaped ESC colony morphology. FGFR inhibition (FGFRi) by SU5402 had little effect compared with LIF (Figure 1A). A two-inhibitor combination (PD0325901 and CHIR99021) and a three-inhibitor combination (PD0325901, CHIR99021, and SU5402) produced robust AP staining of ESCs with a compact colony morphology.

Changes in histone H3 methylation status affect gene expression patterns in a variety of cells (Black et al., 2012). We therefore investigated whether H3K9me3 status is altered by three small-molecule inhibitors. Neither GSK3i nor FGFRi had any effects on H3K9me3 levels, but MEKi reduced H3K9me3 levels. Likewise, 2i (MEKi/GSK3i) decreased H3K9me3 levels (Figure 1B). Interestingly, protein levels of JMJD2C, which is a histone H3K9me3-, H3K9me2-, and H3K36me3-specific histone demethylase (Cloos et al., 2006; Klose et al., 2006; Whetstine et al., 2006), were increased by MEKi after 48 hr (Figure 1B). MEKi also decreased H3K9me2 and H3K36me3 levels (Figures 1C and S1), suggesting that MEKi might keep low H3K9me2/3 levels by the increased JMJD2C levels.

The MAPK/ERK pathway delivers an intracellular signaling by successive kinase reactions, RAS-RAF-MEK-ERK. Therefore, the MEK1/2 inhibitor PD0325901 suppresses MEK1/2 activity, successively reducing downstream ERK1/2 activity. The observation made with PD0325901 could be due to the inhibition of either MEK1/2 or ERK1/2. Therefore, we used the ERK selective inhibitor FR180204 to determine which kinase is responsible for decreasing H3K9me3 levels. Indeed, MEKi, but not ERKi specifically decreased H3K9me3 levels (Figure 1D), indicating that PD0325901-mediated H3K9me3 reduction originates from the selective inhibition of MEK1/2 activity, but not that of ERK1/2 activity.

We used GEO: GSE43597 in the GEO DataSet to explore alterations in gene expression profiles caused by 2i treatments (Zhang et al., 2013). Although the 2i treatment did not alter the expression of most genes in the dataset (Figure 1E and Table S1), it reduced the transcript levels of *Dnmt3a*, *Dnmt3b*, *Dnmt3l*, and *Tet1*, and increased the transcript levels of *Prdm14*, *Prdm1*, *Klf2*, and *Nanog*. Because MEKi resulted in high JMJD2C protein levels (Figure 1B), we examined *Jmjd2c* transcript levels by qRT-PCR. MEKi did not significantly change the transcript levels of *Oct4* but increased those of *Sox2* and decreased those of *Jmjd2c* (Figure 1F). We next examined the protein levels in MEKi-treated ESCs (Figure 1G). MEKi increased OCT4 protein levels, probably by increasing OCT4 protein stability, and SOX2 protein levels, probably by transcriptional induction. MEKi also increased JMJD2C, suggesting the presence of a post-translational modification. Together, our results demonstrate that MEKi increases JMJD2C levels that reduce the repressive H3K9me3 marks at the promoter regions of pluripotent genes in ESCs.

MEK1 Phosphorylates JMJD2C to Promote Ubiquitin-Mediated Protein Degradation

We examined whether MEK1 affects JMJD2C activity via phosphorylation. Purified GST-MEK1 interacted with endogenous JMJD2C directly in ESC lysate (Figure 2A). Because MEK1 is a Ser/Thr and Tyr dual-specificity kinase (Roskoski, 2012), we examined whether MEK1 phosphorylates JMJD2C directly. When we used anti-phosphoserine/threonine antibody to detect phospho-JMJD2C, we did not detect any positive signal (data not shown). An anti-phosphotyrosine 4G10 antibody produced a strong positive signal (Figure 2B), supporting the idea that JMJD2C is a substrate of MEK1 and undergoes phosphorylation at Tyr residues.

JMJD2C consists of four domains, including jumonji N (JmjN) (amino acids 1–140), JmjC (amino acids 141–310), 2×plant homeodomain (PHD) (amino acids 671–868), and 2×TUDOR (amino acids 869–1,054). GST-MEK1 was associated with four mutants containing JmjN, JmjC, 2×PHD, and 2×TUDOR, respectively (Figure 2C). MEK1 phosphorylates a consensus motif containing the amino acid sequence T-X-Y (Cacace et al., 1999). To determine which Tyr residues of JMJD2C are phosphorylated by MEK1, we searched for T-X-Y motifs within JMJD2C. We identified a highly conserved T-P-Y motif at residues 175–177 in the JmjC domain (Figure 2D), which was specifically phosphorylated by MEK1 (Figure 2E). MEK1 phosphorylated the wild-type JmjC domain but not the Y177F mutant JmjC domain (Figure 2F), indicating that Mek1 phosphorylates Y177.

(D) The Y177 residue in JMJD2C is a putative site for phosphorylation by MEK1.
(E and F) In vitro MEK1 kinase assays show that (E) MEK1 phosphorylates the JmjC domain in JMJD2C, and (F) MEK1 phosphorylates wild-type JmjC but not Y177F mutant JmjC. The red asterisk indicates a phosphorylated domain by MEK1.
(G) MEK1 expression increases JMJD2C ubiquitination, but MEKi by PD0325901 suppresses JMJD2C ubiquitination.
(H) MEK1 increases the ubiquitination of wild-type JMJD2C but not Y177F mutant JMJD2C.
(I) MEK1 increases wild-type JmjC ubiquitination.
(J) In the presence of endogenous MEK1, Y177F mutant JmjC is not ubiquitinated compared with wild-type JmjC.

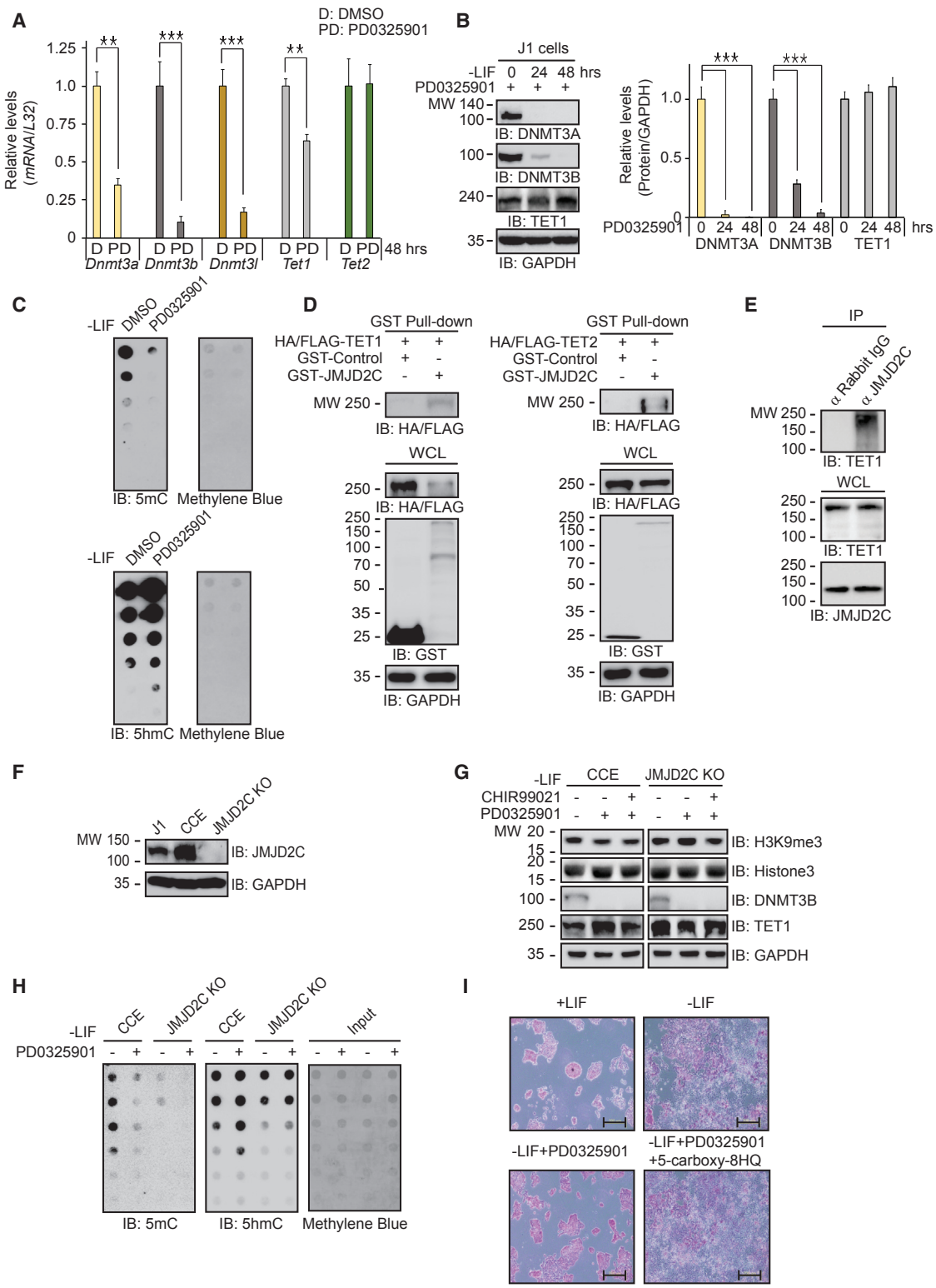

Figure 3. MEK Inhibition Leads to a Decrease of 5mC Levels and an Increase of 5hmC Levels via DNMT3A/B Reduction and JMJD2C-Mediated TET1 Activation, Respectively

(A) qRT-PCR (n = 4 independent experiments) shows that compared with DMSO control, PD0325901 decreases transcript levels of the *Dnmt3* family and *Tet1* but does not change *Tet2* expression. ESCs were cultured in feeder-free and LIF-free conditions with PD0325901 for 48 hr.

(legend continued on next page)

In line with the observation that MEKi increases JMJD2C protein levels (Figure 1G), the MEK1 expression increased JMJD2C ubiquitination, whereas PD0325901 suppressed that effect (Figure 2G). Moreover, the wild-type JMJD2C was more intensely ubiquitinated than a non-phospho mutant, Y177F JMJD2C, by MEK1 (Figure 2H). MEK1 expression increased the ubiquitination of wild-type GST-JmjC (Figure 2I). Likewise, endogenous MEK1/2 ubiquitinated the wild-type JmjC mutant more than the Y177F JmjC mutant (Figure 2J). Collectively, our results support the conclusion that Y177 is a phosphodegron for JMJD2C degradation.

MEKi Decreases DNA Methylation Levels via DNMT3A/B Reduction and Increases DNA Hydroxymethylation Levels via JMJD2C-Associated TET1 Activation

Accumulating evidence suggests that ESCs cultured in 2i/LIF have genome-wide DNA hypomethylation compared with ESCs cultured in serum/LIF (Leitch et al., 2013; Marks and Stunnenberg, 2014). The activities of two opposing enzyme families, DNMT and TET, govern genome-wide methylation. PD0325901-treated ESCs had low transcript levels of *Dnmt3* family and *Tet1*, but unchanged transcript levels of *Tet2* (Figure 3A). PD0325901 seemed to increase TET1 protein levels (Figure 3B), suggesting post-translational modification (Bauer et al., 2015; Chen et al., 2013b; Yu et al., 2013). Consistent with the reductions in transcript levels, DNMT3A/B protein levels were also decreased (Figure 3B), suggesting that MEKi-induced DNMT3A/B reduction is in part due to transcriptional suppression.

DNMT3A/B regulate self-renewal in some stem cells by de novo DNA methylation (Tadokoro et al., 2007; Tsumura et al., 2006). We measured DNA methylation levels by dot-blot assay. Consistent with previous results (Leitch et al., 2013; Marks and Stunnenberg, 2014), MEKi significantly reduced 5mC levels while increasing 5hmC levels (Figure 3C), suggesting that JMJD2C associates with TET1 to enhance methylcytosine dioxygenase activity. Both TET1 and TET2 interacted with JMJD2C (Figure 3D). A co-immunoprecipitation experiment showed that JMJD2C bound to TET1 in ESCs (Figure 3E). Moreover, JMJD2C bound to the catalytic domain of TET1 (Figure S2).

JMJD2C Deficiency Disrupts ESC Pluripotency through Aberrant Methylation of DNA and Histones

We generated *Jmjd2c* knockout (KO) ESCs to study how JMJD2C is involved in the TET1-mediated DNA demethylation pathway (Figure S3). Wild-type ESCs (J1 and CCE) expressed endogenous JMJD2C, whereas *Jmjd2c* KO cells did not express JMJD2C proteins (Figure 3F). We examined whether JMJD2C deficiency influences the 2i-mediated maintenance of a ground state. When parental CCE and *Jmjd2c* KO cells were treated with PD0325901 alone or with 2i, the H3K9me3 levels were decreased in the CCE cells but not in the *Jmjd2c* KO cells (Figure 3G). Nonetheless, both PD0325901 alone and 2i decreased DNMT3B levels in both CCE and *Jmjd2c* KO cells, indicating that DNMT3 expression is independent of JMJD2C. Unlike *Tet1* transcript levels, TET1 protein levels were increased in both CCE cells and *Jmjd2c* KO cells in response to PD0325901 (Figure 3G). Consistent with those results (Figure 3C), MEKi decreased 5mC levels in both CCE cells and *Jmjd2c* KO cells (Figure 3H, see 5mC). In contrast, MEKi increased 5hmC levels in CCE cells but not in *Jmjd2c* KO cells (Figure 3H, see 5hmC), indicating that active TET1-mediated DNA demethylation requires JMJD2C. In addition, the specific JMJD2 inhibitor 5-carboxyl-8-HQ abolished the MEKi-mediated AP staining and ESC-like colony morphology (Figure 3I).

GSK3 Inhibition Decreases 5mC Levels through DNMT3A/B Reduction

We next elucidated the molecular mechanism underlying the maintenance of a ground state in ESCs by GSK3i, which sustains the naive state by activating Wnt signaling (Miki et al., 2011; Wray and Hartmann, 2012). GSK3i decreased

(B) PD0325901 decreases DNMT3A/B protein levels but increases TET1 protein levels in ESCs cultured in feeder-free and LIF-free conditions (n = 3 independent experiments).
(C) Dot blots show that PD0325901 decreases 5mC levels but increases 5hmC levels in ESCs cultured in feeder-free and LIF-free conditions with PD0325901 for 48 hr.
(D) JMJD2C interacts with TET1 and TET2 in a pull-down assay.
(E) JMJD2C associates with TET1 in ESCs in a co-immunoprecipitation experiment.
(F) *Jmjd2c*-KO ESCs do not express endogenous JMJD2C compared with wild-type ESCs.
(G) PD0325901 and/or CHIR99021 decrease DNMT3B levels, but not H3K9me3 levels, in *Jmjd2c* KO cells compared with control CCE cells. ESCs were cultured in feeder-free and LIF-free conditions.
(H) Dot blots show that JMJD2C deficiency leads to reduction of 5mC levels by PD0325901 in both control and *Jmjd2c*-KO ESCs. On the contrary, 5hmC levels are unchanged in *Jmjd2c*-KO ESCs compared to the control cells.
(I) AP staining shows that the specific JMJD2 inhibitor 5-carboxyl-8-HQ disrupts the pluripotent state induced by PD0325901. Scale bar, 200 μm.
**$p < 0.01$ and ***$p < 0.001$.

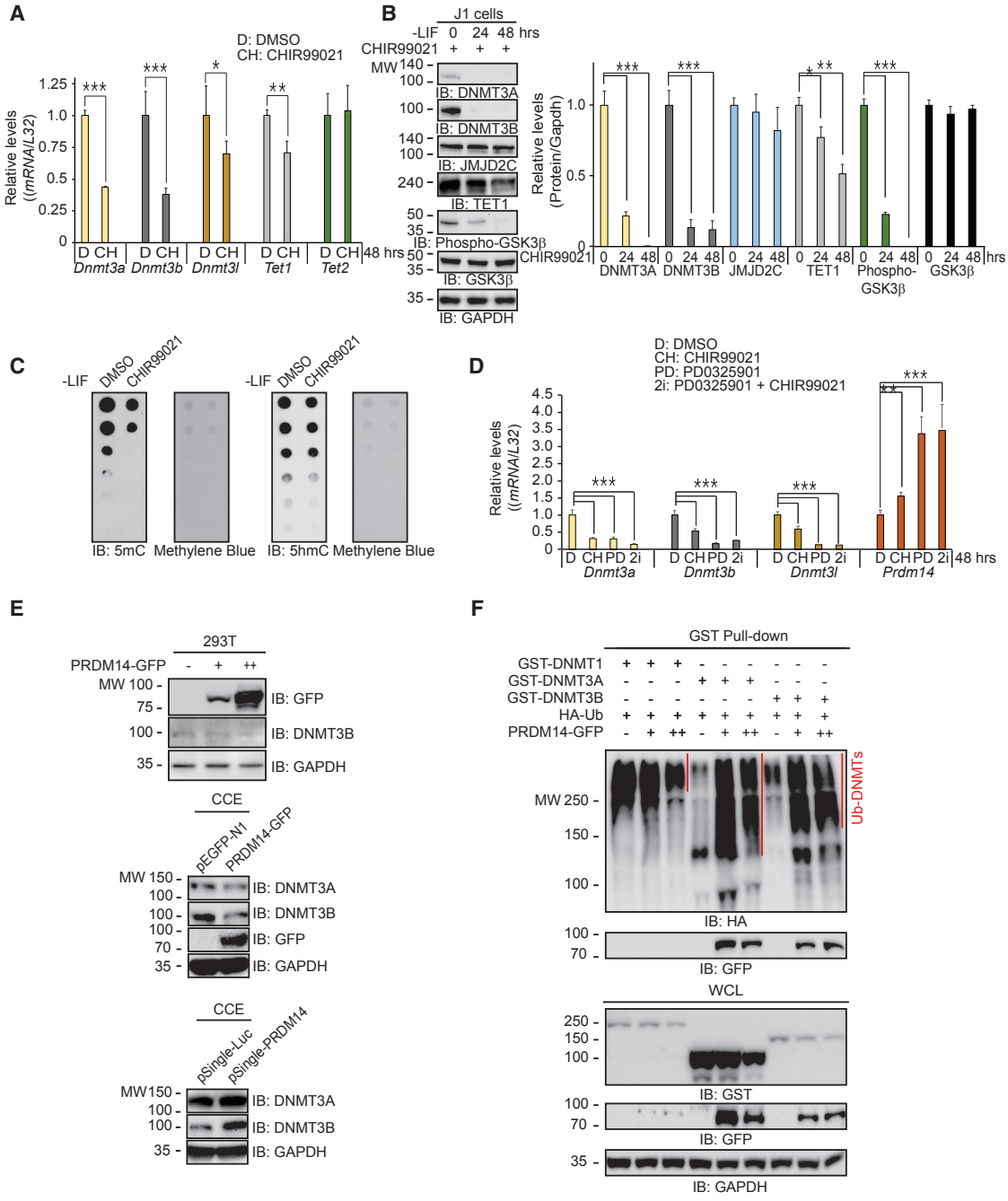

Figure 4. GSK3 Inhibition Decreases 5mC Levels, but Not 5hmC Levels, through Passive DNA Demethylation

(A) qRT-PCR (n = 4 independent experiments) shows that GSK3 inhibition by CHIR99021 decreases transcript levels of the *Dnmt3* family and *Tet1*, but does not alter *Tet2* transcript levels compared with the DMSO control.

(B) Western blots show that CHIR99021 reduces DNMT3A/B and TET1 protein levels without changing JMJD2C levels (n = 3 independent experiments).

(C) Dot blots show that CHIR99021 decreases 5mC levels, but not 5hmC levels, in ESCs cultured in feeder-free and LIF-free conditions with CHIR99021 for 48 hr.

(D) qRT-PCR (n = 4 independent experiments) shows that the 2i treatments upregulate *Prdm14* transcript levels.

(legend continued on next page)

the transcript and protein levels of the DNMT3 family (Figures 4A and 4B). GSK3α/β and MEK1/2 are involved in disparate signaling pathways; however, our data demonstrate that they have partly shared effects, because GSK3i also suppressed *Dnmt3* levels. In contrast, GSK3i downregulated *Tet1* transcription in addition to decreasing TET1 protein levels. In contrast to the effect of MEKi, GSK3i modestly decreased JMJD2C protein levels (Figures 1B and 4B). GSK3i decreased global DNA methylation levels without altering DNA hydroxymethylation levels (Figure 4C), suggesting that GSK3i-mediated DNA hypomethylation results partly from the downregulation of DNMT3 expression.

PRDM14 Downregulates DNMT3A/B Protein Expression

To find a factor that accelerates DNMT3A/B protein degradation, we examined GEO: GSE43597 in the GEO DataSet (Figure 1E and Table S1). Among the genes altered by the 2i conditions, PRDM14 is unique, because it was identified as a key regulator for maintaining ESC pluripotency (Yamaji et al., 2013). Other studies showed that PRDM14 downregulates *Dnmt3* expression (Grabole et al., 2013; Hackett et al., 2013a; Yamaji et al., 2013). Consistent with those observations, all combinatorial 2i treatments increased *Prdm14* expression but decreased *Dnmt3* family expression (Figure 4D).

We investigated the role of PRDM14 to see if it facilitates DNMT3A/B protein degradation. PRDM14 expression in 293T cells decreased endogenous DNMT3B protein levels in a dose-dependent fashion (Figure 4E, upper panel), implying that PRDM14 downregulates DNMT3B by translational control. Similarly, PRDM14 overexpression in ESCs significantly decreased DNMT3A/B protein levels (Figure 4E, middle panel). Conversely, *Prdm14* knockdown by small hairpin RNA (shRNA) upregulated DNMT3A/B protein levels (Figures 4E and S4A), indicating that PRDM14 downregulates DNMT3A/B expression.

Because PRDM14 decreases the expression of *Dnmt3a/b*, but not that of *Dnmt1* (Grabole et al., 2013; Yamaji et al., 2013), we examined the possibility that PRDM14 reduces DNMT3A/B protein levels by promoting ubiquitination-dependent degradation. PRDM14 increased the ubiquitination of DNMT3A/B, but not that of DNMT1 (Figure 4F, see IB: HA). Consistent with that observation, exogenous PRDM14 bound to DNMT3A/B, but not to DNMT1 (Figure 4F, see IB: GFP), indicating that DNMT3A/B protein degradation requires a direct interaction between PRDM14 and DNMT3A/B. Endogenous PRDM14 associated with DNMT3A (Figure S4B) and DNMT3B (Figure S4C). Taken together, our findings strongly indicate that PRDM14 is a key factor in the repression of DNMT3A/B expression and the control of the ESC ground state.

PRDM14 Has G9a Methyltransferase Activity toward DNMT3A/B

We predicted that PRDM14 contains methyltransferase activity toward the DNMT family because of the presence of a PR domain that is a modified version of the HMT SET domain. Contrary to our expectation, PRDM14 did not have obvious methyltransferase activity toward the DNMT family (Figure 5A). We detected only non-specific signals, which we speculated were due to endogenous G9a bound to the DNMT proteins. As expected, PRDM14 interacted with endogenous G9a in an immunoprecipitation assay (Figure 5B) and a pull-down assay (Figure S5).

Recently, we reported that G9a activates MYOD protein degradation in a methylation-dependent manner (Jung et al., 2015). We examined whether G9a activates DNMT3A/B protein degradation. The extent of DNMT3A2 ubiquitination was dependent on G9a > PRDM14 > control > PRDM1 expression (Figure 5C, see IB: HA). We detected an association of DNMT3A2 with PRDM14 and G9a, but not with PRDM1 (Figure 5C, see IB: GFP/GST). We observed the similar associations for DNMT3B (Figure S6A). Overall, the degree of PRDM14-mediated DNMT3A/B ubiquitination was lower than that of G9a-mediated DNMT3A/B ubiquitination, suggesting that PRDM14-mediated DNMT3A/B degradation is required for G9a recruitment to the PRDM14/DMNT3A/B complex in ESCs.

G9a inhibition attenuates PRDM14-mediated DNMT3/B degradation. The G9a-specific inhibitor UNC0638 suppressed PRDM14-mediated DNMT3A/B degradation (Figures 5D and S6B). Likewise, *G9a* silencing by shRNA decreased DNMT3A/B ubiquitination (Figures 5E and S6C). The 2i culture conditions induced a high level of *Prdm14* expression (Figures 1E and 4D). Therefore, we hypothesized that PRDM14 functions as a scaffold to aid the assembly between DNMT3A/B and G9a. To address that, we used the mouse 248-5 ESC line, which does not express G9a and G9a-like protein (GLP). Compared with wild-type TT2 cells, the 248-5 cells exhibited alterations in the 2i-

(E) PRDM14 expression in 293T cells decreases DNMT3B levels in a dose-dependent fashion (top panel). PRDM14 expression in ESCs decreases DNMT3A/B levels in ESCs (middle panel). Knockdown of *Prdm14* by shRNA increases DNMT3A/B levels in ESCs (bottom panel).
(F) GST pull-down assays show that PRDM14 expression increases the ubiquitination of DNMT3A/B through protein-protein interactions; PRDM14 does not increase DNMT1 ubiquitination.
*$p < 0.05$, **$p < 0.01$, and ***$p < 0.001$.

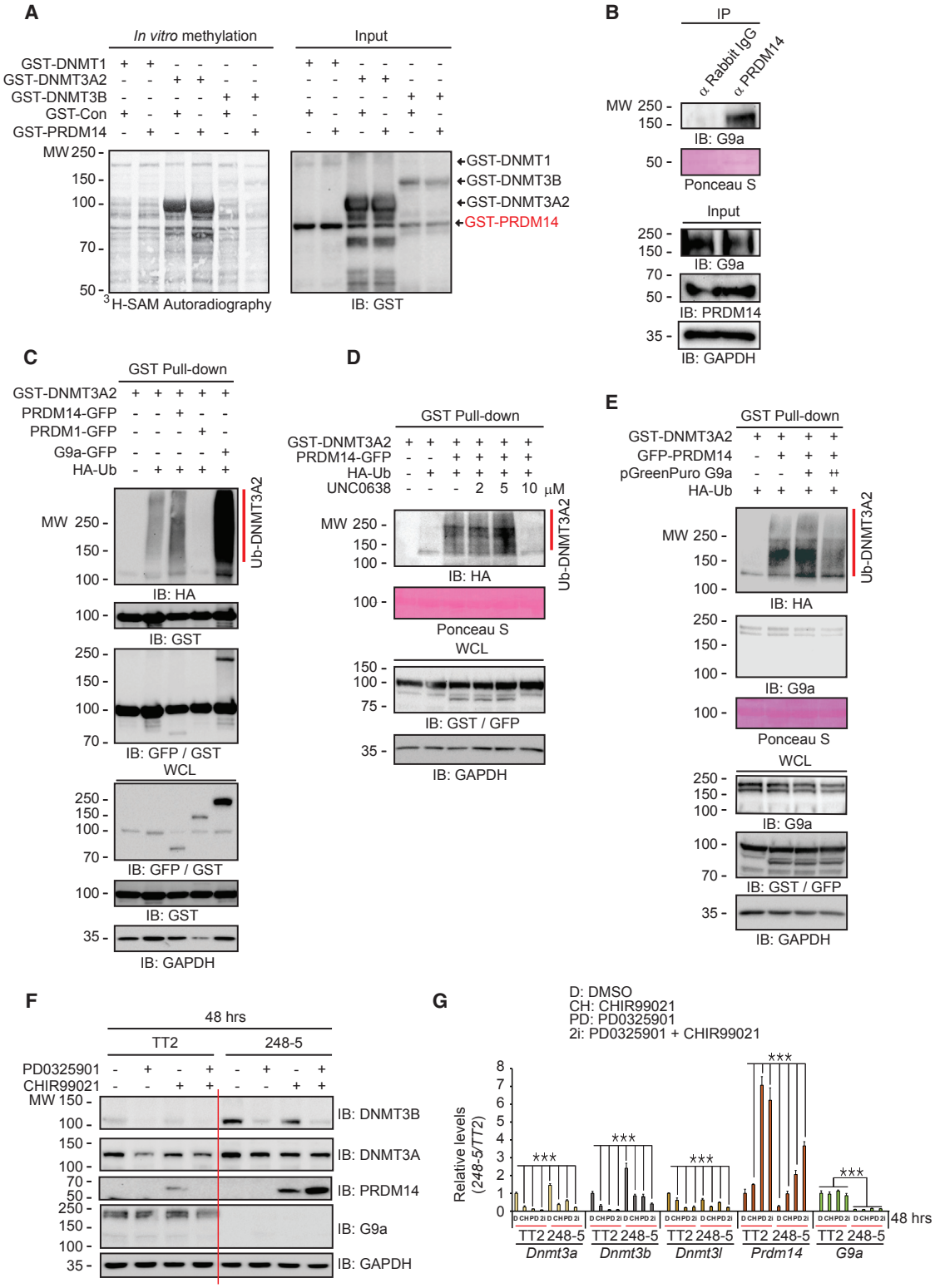

Figure 5. PDRM14-Mediated G9a/DNMT3A Complex Formation Promotes DNMT3A Protein Degradation

(A) DNMT1, DNMT3A2, and DNMT3B in vitro PRDM14 methyltransferase assay shows that PRDM14 has no methyltransferase activity toward the DNMT family.

(B) Immunoprecipitation assay shows that endogenous PRDM14 associates with G9a.

(legend continued on next page)

mediated reduction of DNMT3A/B and induction of PRDM14 determined by the express levels of proteins (Figure 5F) and mRNAs (Figure 5G), suggesting that PRDM14-mediated DNMT3 protein degradation requires G9a and GLP recruitment. Taken together, our results show that PRDM14 does not have methyltransferase activity; however, it serves as a scaffold to promote DNMT3A/B protein degradation by G9a.

G9a Methylates DNMT3A/B

The DNMT3A family consists of the DNMT3A and DNMT3A2 isoforms. *Dnmt3a2* transcription is initiated from a downstream intronic promoter. As a result, DNMT3A2 lacks the 219 N-terminal amino acid residues of the full-length protein (Chen et al., 2002). The K44 residue in DNMT3A is a G9a methylation site (Chang et al., 2011). Although DNMT3A2 lacks the K44 residue, G9a methylated DNMT3A2, DNMT3B, and DNMT1 (Figure 6A), indicating the presence of another methylation site besides K44 in DNMT3A.

To determine potential methylation sites in DNMT3A2, we conducted an in vitro G9a methyltransferase assay. G9a methylated full-length DNMT3A2 and an N-terminal mutant $DNMT3A2_{126\text{-}250}$ (Figure 6B). Similarly, G9a methylated full-length DNMT3B as well as an N-terminal mutant, $DNMT3B_{241\text{-}340}$ (Figure 6C). The PWWP domain in DNMT3A, DNMT3A2, and DNMT3B contains a conserved G9a methylation motif with RK residues (Figure 6E). As anticipated, G9a only methylated a GST-fusion protein containing the PAKKPRKSTTEKP residues in DNMT3A2 (Figure 6D). Collectively, our data show that G9a methylates DNMT3A/B, and the PWWP domain in DNMT3A/B is a G9a methylation site. Those findings contradict a previous report that K44 in full-length DNMT3A is the sole residue methylated by G9a (Chang et al., 2011).

G9a/GLP Promotes DNMT3A/B Degradation through Methylation-Dependent Ubiquitination

GLP belongs to the same family of histone lysine N-methyltransferases as G9a (Shinkai and Tachibana, 2011). Therefore, we expected GLP to increase DNMT3A2 ubiquitination. Indeed, GLP increased DNMT3A2 ubiquitination similarly to G9a (Figure 7A), indicating that G9a and GLP facilitate DNMT3A2 and DNMT3B ubiquitination in a methylation-dependent manner. The G9a/GLP inhibitor UNC0638 decreased DNMT3A2 ubiquitination (Figure 7B) and increased DNMT3A protein levels in a dose-dependent fashion (Figure 7C). Likewise, UNC0638 increased 5mC levels (Figure 7D). The silencing of endogenous *G9a* by shRNAs resulted in an increase of DNMT3A protein levels concomitant with a reduction of G9a levels (Figure S7A), indicating that DNMT3A protein levels are regulated by methylation status. In 248-5 cells, DNMT3A and DNMT3A2 levels were elevated compared with those in control TT2 cells (Figures 5F and S7B). Overall, our results strongly suggest that G9a/GLP regulates global DNA methylation status through DNMT3A/B protein degradation.

DISCUSSION

ESCs cultured in 2i/LIF exhibit unique features including the elevated expression of pluripotent genes, the suppression of genes mediating cell differentiation, and global DNA hypomethylation. Thus, 2i ESCs sustain a ground state of pluripotency similar to that of the ICM. To elucidate the molecular mechanism by which 2i (MEKi/GSK3i) maintains a naive ground state in ESCs, we devised a treatment method of MEKi and GSK3i, both separately and in combination, without LIF. This approach allowed us to uncover that MEKi increased JMJD2C protein levels, thereby enhancing TET1 activity, whereas GSK3i decreased DNMT3 family expression. Our results clearly demonstrate that active and passive DNA demethylation pathways under 2i conditions are governed by the JMJD2C/TET and PRDM14/G9a/DNMT3 complexes, respectively.

A recent series of findings indicated that DNA methylation in 2i ESCs correlates with H3K27me3 (Marks et al., 2012) and H3K9me3 levels (Habibi et al., 2013). JMJD2C is an HDM specific for H3K9me3, H3K9me2, and H3K36me3 (Cloos et al., 2006; Klose et al., 2006; Whetstine et al., 2006), and plays important roles in the maintenance of self-renewal and pluripotency in ESCs (Das et al., 2014; Loh et al., 2007; Pedersen et al., 2014; Wang et al., 2010). MEKi increased JMJD2C protein levels, which was accompanied with H3K9me3 reduction and downregulated *Jmjd2c* transcript levels, indicating the existence of a post-translational modification.

(C) DNMT3A2 ubiquitination is proportional to the expression of G9a > PRDM14 > Control > PRDM1.
(D) PRDM14 increases DNMT3A2 ubiquitination, but UNC0638 inhibits PRDM14-mediated DNMT3A2 degradation.
(E) Knockdown of endogenous *G9a* by the shRNA decreases PRDM14-mediated DNMT3A2 ubiquitination.
(F and G) Knockout of *G9a* and *GLP* disrupts 2i-mediated reduction of DNMT3A/B and induction of PRDM14 determined by (F) western blots and (G) qRT-PCR (n = 4 independent experiments) in G9a and GLP double-knockout 248-5 ESCs compared with control TT2 cells. ***$p < 0.001$.

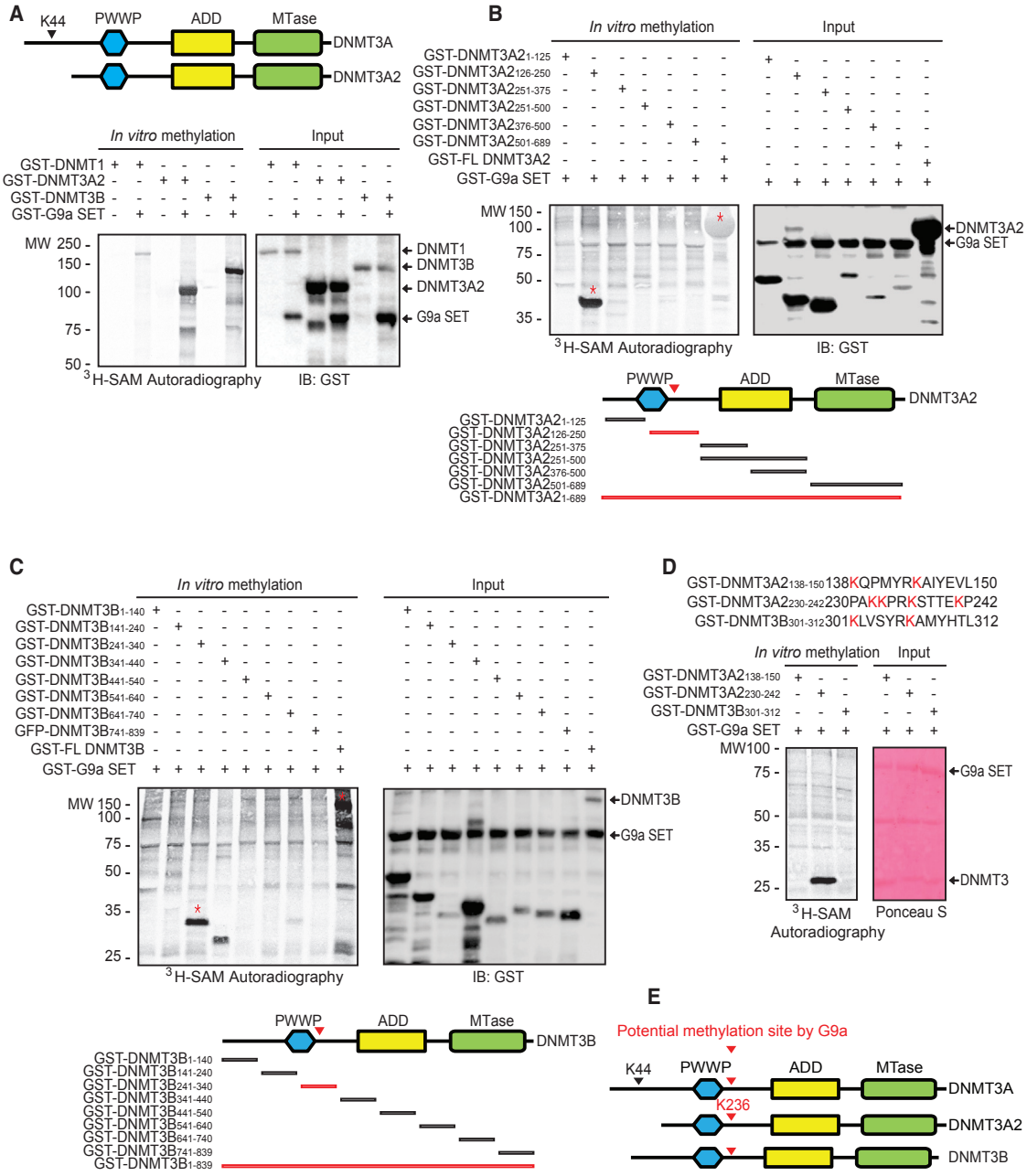

Figure 6. G9a Directly Methylates DNMT3A2, DNMT3B, and DNMT1

(A) In vitro G9a methyltransferase assay shows that G9a methylates DNMT3A2, DNMT3B, and DNMT1. G9a also methylates DNMT3A2, an alternative splicing form, which lacks the K44 residue.

(B–D) In vitro G9a methyltransferase assay shows that G9a methylates (B) the region of amino acids 126–250 in DNMT3A2, (C) the region of amino acids 241–340 in DNMT3B, and (D) lysine residues at the consensus RK methylation site in DNMT3A2 and DNMT3B. The red asterisks are the methylated proteins.

(E) A schematic diagram of potential sites for methylation by G9a in DNMT3A, DNMT3A2, and DNMT3B.

Because MEK1/2 is a dual-specificity kinase (Roskoski, 2012), there must be a T-X-Y motif present in JMJD2C. We identified a T-P-Y motif in the JmjC domain. Our findings attribute the phosphorylation of full-length JMJD2C by MEK1 to the presence of the T-P-Y motif in the JmjC domain. The phosphorylation of some proteins is coupled to protein degradation through ubiquitination (Huang et al., 2012; Hunter, 2007; Swaney et al., 2013). Hence,

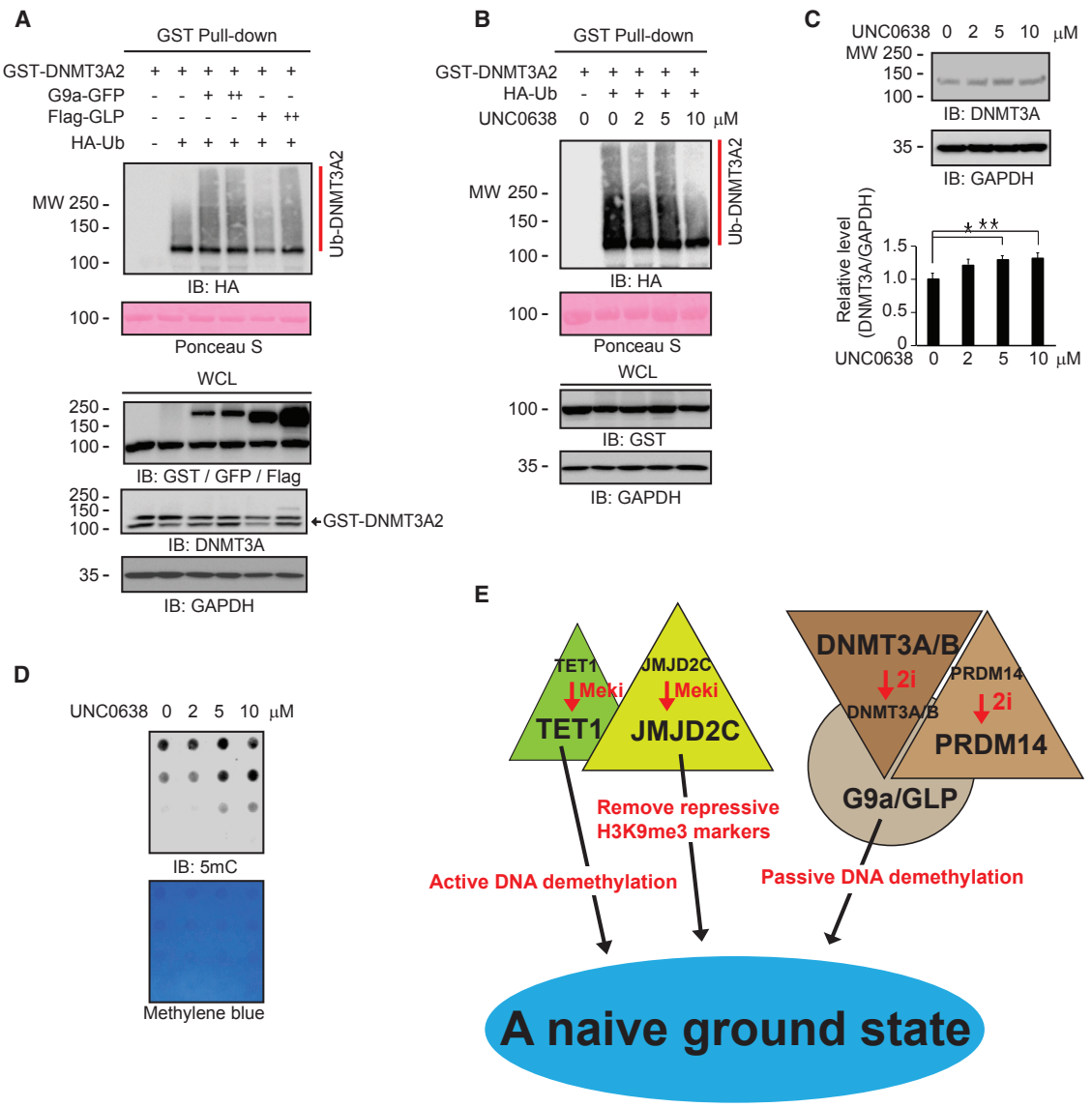

Figure 7. G9a and GLP Control DNMT3 Degradation in a Methylation-Dependent Manner

(A and B) GST pull-down assays show that (A) GLP and G9a play a key role in DNMT3A2 ubiquitination, and (B) G9a inhibition by the G9a/GLP inhibitor UNC0638 decreases DNMT3A2 ubiquitination.

(C) Western blots show that UNC0638 increases endogenous DNMT3A protein levels in a dose-dependent manner (n = 3 independent experiments).

(D) Dot blots show that G9a inhibition by UNC0638 increases DNA methylation levels.

(E) A model showing that the 2i condition maintains ESCs in a naive ground state through two axes of distinct protein complexes: JMJD2C-enhanced TET1 potentiation and PRDM14/G9A-dependent DNMT3A/B protein degradation.

*$p < 0.05$ and **$p < 0.01$.

the phosphorylation of the Y177 residue in the T-P-Y motif of JMJD2C may play a role in recruiting an unknown E3 ligase to degrade JMJD2C. MEK1 expression increased JMJD2C ubiquitination; however, MEKi suppressed JMJD2C ubiquitination. The Y177F mutant JMJD2C was less ubiquitinated than wild-type JMJD2C in the presence of MEK1. Therefore, we propose that Y177 is a phosphodegron for JMJD2C protein degradation in ESCs.

We speculated that MEKi might decrease DNA methylation levels through the downregulation of the DNMT3 family. MEKi significantly diminished global DNA methylation levels and, surprisingly, was sufficient to induce high 5hmC levels. Because the TET family of dioxygenases that

catalyze the conversion of 5mC into 5hmC plays important roles in the induction of DNA hypomethylation (Hill et al., 2014; Kohli and Zhang, 2013), we hypothesized that JMJD2C might interact with TET family members. Thus, the absence of *Jmjd2c* may disrupt MEKi-induced DNA hydroxymethylation. Indeed, when *Jmjd2c* was knocked out, 5hmC levels were not altered by MEKi, suggesting that TET1 activity toward 5mC requires JMJD2C. Consequently, MEKi decreases 5mC levels via DNMT3A/B reduction and increases 5hmC levels via the enhancement of TET1 activity. Our findings support the idea that MEKi promotes a ground state in ESCs by lowering global DNA methylation through two different mechanisms: passive DNA demethylation via reduction of the DNMT3 family and active DNA demethylation via JMJD2C-mediated TET1 activation.

GSK3i reduced *Dnmt3* family transcript levels, thus decreasing DNMT3A/B protein levels. Remarkably, GSK3i decreased global 5mC levels without altering 5hmC levels, indicating that GSK3i regulates DNA demethylation by a mechanism different than that of MEKi. Thus, our results show that GSK3i-induced DNA demethylation does not involve active DNA demethylation by the TET family.

PRDM14 regulates the maintenance of naive pluripotency in ESCs through a dual mechanism: the inhibition of FGFR signaling and the repression of *Dnmt3* expression (Grabole et al., 2013; Hackett et al., 2013a; Yamaji et al., 2013). Although PRDM14 contains a PR/SET domain, we could not detect PRDM14 methyltransferase activity toward the DNMT family. Instead, we discovered that G9a interacts with PRDM14. Consistent with recent reports (Grabole et al., 2013; Hackett et al., 2013a; Yamaji et al., 2013), PRDM14 suppressed the expression levels of DNMT3A/B and, moreover, interacted with DNMT3A/B but not with DNMT1. G9a interacted with and methylated the DNMT3 family. Based on those findings, we postulated that PRDM14 might serve as a scaffold to accommodate both G9a and DNMT3A/B and facilitate G9a-mediated DNMT3A/B protein degradation when PRDM14 is strongly induced in ESCs under 2i/LIF conditions. In accordance with that idea, DNMT3A/B levels in *G9a*/*GLP* double-KO cells were high under normal conditions and were less affected than those in wild-type cells under 2i conditions. We propose that DNMT3A/B methylation by G9a leads to the degradation of those proteins through a mechanism similar to the one we reported previously (Jung et al., 2015). Therefore, DNMT3A/B may contain a methyl degron targeted by G9a. This idea is supported by our findings that 248-5 cells express high levels of DNMT3A/B mRNA and protein compared with wild-type TT2 cells.

MEK1/2 and GSK3α/β could have many phosphorylation targets in ESCs. Thus, we focused on the roles of targets changed by PD0325901 and CHIR99021. However, researchers have largely ignored protein modifications induced by 2i thus far. 2i may affect the protein and mRNA levels of those targets differently, as we observed with JMJD2C, OCT4, and TET1. In agreement with that conclusion, UHRF1 was decreased on the protein level during the serum-to-2i transition (von Meyenn et al., 2016). We could discriminate between the effects of the inhibitors, either alone or in combination, on transcriptional and translational control; thus, the DNMT3 family was reduced by 2i through transcriptional suppression and protein degradation. Our findings suggest that PD0325901 alone might be sufficient to maintain a ground state in ESCs. Likewise, PD0325901 alone induced the formation of PGC-like cells from ESCs (Kimura et al., 2014). But, CHIR99021 alone sustained an ESC-like morphology (Figure 1A), probably due to suppression of Wnt signaling (Atlasi et al., 2013). Thus, the combination of MEKi and GSK3i must have a synergistic effect on the maintenance of ESCs in a naive ground state. Taken together, our data support a model wherein 2i maintains the ground state in ESCs through JMJD2C-enhanced TET1 activation and PRDM14/G9a-dependent DNMT3A/B protein degradation (Figure 7E).

EXPERIMENTAL PROCEDURES

Cell Culture

The mouse ESC lines J1 (ATCC SCRC-1010), CCE, and *Jmjd2c* KO were used.

AP Staining

For AP staining, ESCs were washed twice with PBS and fixed them with 4% paraformaldehyde for 5 min at room temperature. We performed staining using the Leukocyte Alkaline Phosphatase Kit (Sigma-Aldrich, 86R) according to the manufacturer's protocol.

Statistics

We presented data as the mean ± SEM. We used GraphPad Prism 6 software to perform Student's t tests for parametric data to compare groups. In the figures, *$p < 0.05$, **$p < 0.01$, and ***$p < 0.001$ denote the statistical significance.

SUPPLEMENTAL INFORMATION

Supplemental Information includes Supplemental Experimental Procedures, seven figures, and two tables and can be found with this article online at http://dx.doi.org/10.1016/j.stemcr.2017.04.001.

AUTHOR CONTRIBUTIONS

C.K. conceived the study; K.K. planned the project; Y.S., Y.Y., and S.K. performed the ESC-related experiments; M.K. and A.N. performed the molecular experiments; K.P., C.K., and K.K. analyzed and interpreted the data; C.K., K.P., and Y.S. wrote the manuscript;

all authors discussed the results and approved the final manuscript for publication.

ACKNOWLEDGMENTS

We are grateful to Dr. Makoto Tachibana for providing mouse TT2 and 248-5 ESCs. This research was supported by the National Research Foundation of Korea (NRF) funded by the Ministry of Science, ICT and Future Planning (no. 2012M3A9B4028738) and the Ministry of Education (no. 2015R1D1A1A01060986).

Received: November 7, 2016
Revised: March 31, 2017
Accepted: April 3, 2017
Published: April 27, 2017

REFERENCES

Atlasi, Y., Noori, R., Gaspar, C., Franken, P., Sacchetti, A., Rafati, H., Mahmoudi, T., Decraene, C., Calin, G.A., Merrill, B.J., et al. (2013). Wnt signaling regulates the lineage differentiation potential of mouse embryonic stem cells through Tcf3 down-regulation. PLoS Genet. *9*, e1003424.

Bagci, H., and Fisher, A.G. (2013). DNA demethylation in pluripotency and reprogramming: the role of tet proteins and cell division. Cell Stem Cell *13*, 265–269.

Bauer, C., Gobel, K., Nagaraj, N., Colantuoni, C., Wang, M., Muller, U., Kremmer, E., Rottach, A., and Leonhardt, H. (2015). Phosphorylation of TET proteins is regulated via O-GlcNAcylation by the O-linked N-acetylglucosamine transferase (OGT). J. Biol. Chem. *290*, 4801–4812.

Baylin, S.B. (2005). DNA methylation and gene silencing in cancer. Nat. Clin. Pract. Oncol. *2* (*Suppl 1*), S4–S11.

Black, J.C., Van Rechem, C., and Whetstine, J.R. (2012). Histone lysine methylation dynamics: establishment, regulation, and biological impact. Mol. Cell *48*, 491–507.

Cacace, A.M., Michaud, N.R., Therrien, M., Mathes, K., Copeland, T., Rubin, G.M., and Morrison, D.K. (1999). Identification of constitutive and ras-inducible phosphorylation sites of KSR: implications for 14-3-3 binding, mitogen-activated protein kinase binding, and KSR overexpression. Mol. Cell Biol. *19*, 229–240.

Chang, Y., Sun, L., Kokura, K., Horton, J.R., Fukuda, M., Espejo, A., Izumi, V., Koomen, J.M., Bedford, M.T., Zhang, X., et al. (2011). MPP8 mediates the interactions between DNA methyltransferase Dnmt3a and H3K9 methyltransferase GLP/G9a. Nat. Commun. *2*, 533.

Chen, T., Ueda, Y., Xie, S., and Li, E. (2002). A novel Dnmt3a isoform produced from an alternative promoter localizes to euchromatin and its expression correlates with active de novo methylation. J. Biol. Chem. *277*, 38746–38754.

Chen, J., Liu, H., Liu, J., Qi, J., Wei, B., Yang, J., Liang, H., Chen, Y., Chen, J., Wu, Y., et al. (2013a). H3K9 methylation is a barrier during somatic cell reprogramming into iPSCs. Nat. Genet. *45*, 34–42.

Chen, Q., Chen, Y., Bian, C., Fujiki, R., and Yu, X. (2013b). TET2 promotes histone O-GlcNAcylation during gene transcription. Nature *493*, 561–564.

Cherepkova, M.Y., Sineva, G.S., and Pospelov, V.A. (2016). Leukemia inhibitory factor (LIF) withdrawal activates mTOR signaling pathway in mouse embryonic stem cells through the MEK/ERK/TSC2 pathway. Cell Death Dis. *7*, e2050.

Cloos, P.A., Christensen, J., Agger, K., Maiolica, A., Rappsilber, J., Antal, T., Hansen, K.H., and Helin, K. (2006). The putative oncogene GASC1 demethylates tri- and dimethylated lysine 9 on histone H3. Nature *442*, 307–311.

Das, P.P., Shao, Z., Beyaz, S., Apostolou, E., Pinello, L., De Los Angeles, A., O'Brien, K., Atsma, J.M., Fujiwara, Y., Nguyen, M., et al. (2014). Distinct and combinatorial functions of Jmjd2b/Kdm4b and Jmjd2c/Kdm4c in mouse embryonic stem cell identity. Mol. Cell *53*, 32–48.

Dillon, S.C., Zhang, X., Trievel, R.C., and Cheng, X. (2005). The SET-domain protein superfamily: protein lysine methyltransferases. Genome Biol. *6*, 227.

Epsztejn-Litman, S., Feldman, N., Abu-Remaileh, M., Shufaro, Y., Gerson, A., Ueda, J., Deplus, R., Fuks, F., Shinkai, Y., Cedar, H., et al. (2008). De novo DNA methylation promoted by G9a prevents reprogramming of embryonically silenced genes. Nat. Struct. Mol. Biol. *15*, 1176–1183.

Esteve, P.O., Patnaik, D., Chin, H.G., Benner, J., Teitell, M.A., and Pradhan, S. (2005). Functional analysis of the N- and C-terminus of mammalian G9a histone H3 methyltransferase. Nucleic Acids Res. *33*, 3211–3223.

Evans, M.J., and Kaufman, M.H. (1981). Establishment in culture of pluripotential cells from mouse embryos. Nature *292*, 154–156.

Grabole, N., Tischler, J., Hackett, J.A., Kim, S., Tang, F., Leitch, H.G., Magnusdottir, E., and Surani, M.A. (2013). Prdm14 promotes germline fate and naive pluripotency by repressing FGF signalling and DNA methylation. EMBO Rep. *14*, 629–637.

Gu, T.P., Guo, F., Yang, H., Wu, H.P., Xu, G.F., Liu, W., Xie, Z.G., Shi, L., He, X., Jin, S.G., et al. (2011). The role of Tet3 DNA dioxygenase in epigenetic reprogramming by oocytes. Nature *477*, 606–610.

Habibi, E., Brinkman, A.B., Arand, J., Kroeze, L.I., Kerstens, H.H., Matarese, F., Lepikhov, K., Gut, M., Brun-Heath, I., Hubner, N.C., et al. (2013). Whole-genome bisulfite sequencing of two distinct interconvertible DNA methylomes of mouse embryonic stem cells. Cell Stem Cell *13*, 360–369.

Hackett, J.A., Dietmann, S., Murakami, K., Down, T.A., Leitch, H.G., and Surani, M.A. (2013a). Synergistic mechanisms of DNA demethylation during transition to ground-state pluripotency. Stem Cell Rep. *1*, 518–531.

Hackett, J.A., Sengupta, R., Zylicz, J.J., Murakami, K., Lee, C., Down, T.A., and Surani, M.A. (2013b). Germline DNA demethylation dynamics and imprint erasure through 5-hydroxymethylcytosine. Science *339*, 448–452.

Hill, P.W., Amouroux, R., and Hajkova, P. (2014). DNA demethylation, Tet proteins and 5-hydroxymethylcytosine in epigenetic reprogramming: an emerging complex story. Genomics *104*, 324–333.

Huang, W., Lv, X., Liu, C., Zha, Z., Zhang, H., Jiang, Y., Xiong, Y., Lei, Q.Y., and Guan, K.L. (2012). The N-terminal phosphodegron targets TAZ/WWTR1 protein for SCFbeta-TrCP-dependent

degradation in response to phosphatidylinositol 3-kinase inhibition. J. Biol. Chem. *287*, 26245–26253.

Hunter, T. (2007). The age of crosstalk: phosphorylation, ubiquitination, and beyond. Mol. Cell *28*, 730–738.

Ito, S., D'Alessio, A.C., Taranova, O.V., Hong, K., Sowers, L.C., and Zhang, Y. (2010). Role of Tet proteins in 5mC to 5hmC conversion, ES-cell self-renewal and inner cell mass specification. Nature *466*, 1129–1133.

Jin, B., Li, Y., and Robertson, K.D. (2011). DNA methylation: superior or subordinate in the epigenetic hierarchy? Genes Cancer *2*, 607–617.

Jung, E.S., Sim, Y.J., Jeong, H.S., Kim, S.J., Yun, Y.J., Song, J.H., Jeon, S.H., Choe, C., Park, K.T., Kim, C.H., et al. (2015). Jmjd2C increases MyoD transcriptional activity through inhibiting G9a-dependent MyoD degradation. Biochim. Biophys. Acta *1849*, 1081–1094.

Kimura, T., Kaga, Y., Ohta, H., Odamoto, M., Sekita, Y., Li, K., Yamano, N., Fujikawa, K., Isotani, A., Sasaki, N., et al. (2014). Induction of primordial germ cell-like cells from mouse embryonic stem cells by ERK signal inhibition. Stem Cells *32*, 2668–2678.

Klose, R.J., Yamane, K., Bae, Y., Zhang, D., Erdjument-Bromage, H., Tempst, P., Wong, J., and Zhang, Y. (2006). The transcriptional repressor JHDM3A demethylates trimethyl histone H3 lysine 9 and lysine 36. Nature *442*, 312–316.

Koh, K.P., Yabuuchi, A., Rao, S., Huang, Y., Cunniff, K., Nardone, J., Laiho, A., Tahiliani, M., Sommer, C.A., Mostoslavsky, G., et al. (2011). Tet1 and Tet2 regulate 5-hydroxymethylcytosine production and cell lineage specification in mouse embryonic stem cells. Cell Stem Cell *8*, 200–213.

Kohli, R.M., and Zhang, Y. (2013). TET enzymes, TDG and the dynamics of DNA demethylation. Nature *502*, 472–479.

Kunath, T., Saba-El-Leil, M.K., Almousailleakh, M., Wray, J., Meloche, S., and Smith, A. (2007). FGF stimulation of the Erk1/2 signalling cascade triggers transition of pluripotent embryonic stem cells from self-renewal to lineage commitment. Development *134*, 2895–2902.

Lei, H., Oh, S.P., Okano, M., Juttermann, R., Goss, K.A., Jaenisch, R., and Li, E. (1996). De novo DNA cytosine methyltransferase activities in mouse embryonic stem cells. Development *122*, 3195–3205.

Leitch, H.G., McEwen, K.R., Turp, A., Encheva, V., Carroll, T., Grabole, N., Mansfield, W., Nashun, B., Knezovich, J.G., Smith, A., et al. (2013). Naive pluripotency is associated with global DNA hypomethylation. Nat. Struct. Mol. Biol. *20*, 311–316.

Ling, B.M., Bharathy, N., Chung, T.K., Kok, W.K., Li, S., Tan, Y.H., Rao, V.K., Gopinadhan, S., Sartorelli, V., Walsh, M.J., et al. (2012). Lysine methyltransferase G9a methylates the transcription factor MyoD and regulates skeletal muscle differentiation. Proc. Natl. Acad. Sci. USA *109*, 841–846.

Loh, Y.H., Zhang, W., Chen, X., George, J., and Ng, H.H. (2007). Jmjd1a and Jmjd2c histone H3 Lys 9 demethylases regulate self-renewal in embryonic stem cells. Genes Dev. *21*, 2545–2557.

Marks, H., and Stunnenberg, H.G. (2014). Transcription regulation and chromatin structure in the pluripotent ground state. Biochim. Biophys. Acta *1839*, 129–137.

Marks, H., Kalkan, T., Menafra, R., Denissov, S., Jones, K., Hofemeister, H., Nichols, J., Kranz, A., Stewart, A.F., Smith, A., et al. (2012). The transcriptional and epigenomic foundations of ground state pluripotency. Cell *149*, 590–604.

Martin, G.R. (1981). Isolation of a pluripotent cell line from early mouse embryos cultured in medium conditioned by teratocarcinoma stem cells. Proc. Natl. Acad. Sci. USA *78*, 7634–7638.

Matsuda, T., Nakamura, T., Nakao, K., Arai, T., Katsuki, M., Heike, T., and Yokota, T. (1999). STAT3 activation is sufficient to maintain an undifferentiated state of mouse embryonic stem cells. EMBO J. *18*, 4261–4269.

Miki, T., Yasuda, S.Y., and Kahn, M. (2011). Wnt/beta-catenin signaling in embryonic stem cell self-renewal and somatic cell reprogramming. Stem Cell Rev. *7*, 836–846.

Miyanari, Y., and Torres-Padilla, M.E. (2012). Control of ground-state pluripotency by allelic regulation of Nanog. Nature *483*, 470–473.

Nakaki, F., and Saitou, M. (2014). PRDM14: a unique regulator for pluripotency and epigenetic reprogramming. Trends Biochem. Sci. *39*, 289–298.

Ng, H.H., and Surani, M.A. (2011). The transcriptional and signalling networks of pluripotency. Nat. Cell Biol. *13*, 490–496.

Niwa, H., Burdon, T., Chambers, I., and Smith, A. (1998). Self-renewal of pluripotent embryonic stem cells is mediated via activation of STAT3. Genes Dev. *12*, 2048–2060.

Okano, M., Bell, D.W., Haber, D.A., and Li, E. (1999). DNA methyltransferases Dnmt3a and Dnmt3b are essential for de novo methylation and mammalian development. Cell *99*, 247–257.

Onishi, K., and Zandstra, P.W. (2015). LIF signaling in stem cells and development. Development *142*, 2230–2236.

Pedersen, M.T., Agger, K., Laugesen, A., Johansen, J.V., Cloos, P.A., Christensen, J., and Helin, K. (2014). The demethylase JMJD2C localizes to H3K4me3-positive transcription start sites and is dispensable for embryonic development. Mol. Cell Biol. *34*, 1031–1045.

Rathert, P., Dhayalan, A., Murakami, M., Zhang, X., Tamas, R., Jurkowska, R., Komatsu, Y., Shinkai, Y., Cheng, X., and Jeltsch, A. (2008). Protein lysine methyltransferase G9a acts on non-histone targets. Nat. Chem. Biol. *4*, 344–346.

Roskoski, R., Jr. (2012). MEK1/2 dual-specificity protein kinases: structure and regulation. Biochem. Biophys. Res. Commun. *417*, 5–10.

Shen, L., Wu, H., Diep, D., Yamaguchi, S., D'Alessio, A.C., Fung, H.L., Zhang, K., and Zhang, Y. (2013). Genome-wide analysis reveals TET- and TDG-dependent 5-methylcytosine oxidation dynamics. Cell *153*, 692–706.

Shinkai, Y., and Tachibana, M. (2011). H3K9 methyltransferase G9a and the related molecule GLP. Genes Dev. *25*, 781–788.

Silva, J., Barrandon, O., Nichols, J., Kawaguchi, J., Theunissen, T.W., and Smith, A. (2008). Promotion of reprogramming to ground state pluripotency by signal inhibition. PLoS Biol. *6*, e253.

Silva, J., Nichols, J., Theunissen, T.W., Guo, G., van Oosten, A.L., Barrandon, O., Wray, J., Yamanaka, S., Chambers, I., and Smith, A. (2009). Nanog is the gateway to the pluripotent ground state. Cell *138*, 722–737.

Smith, A.G., Heath, J.K., Donaldson, D.D., Wong, G.G., Moreau, J., Stahl, M., and Rogers, D. (1988). Inhibition of pluripotential embryonic stem cell differentiation by purified polypeptides. Nature *336*, 688–690.

Smith, Z.D., Chan, M.M., Mikkelsen, T.S., Gu, H., Gnirke, A., Regev, A., and Meissner, A. (2012). A unique regulatory phase of DNA methylation in the early mammalian embryo. Nature *484*, 339–344.

Stavridis, M.P., Lunn, J.S., Collins, B.J., and Storey, K.G. (2007). A discrete period of FGF-induced Erk1/2 signalling is required for vertebrate neural specification. Development *134*, 2889–2894.

Subramaniam, D., Thombre, R., Dhar, A., and Anant, S. (2014). DNA methyltransferases: a novel target for prevention and therapy. Front Oncol. *4*, 80.

Swaney, D.L., Beltrao, P., Starita, L., Guo, A., Rush, J., Fields, S., Krogan, N.J., and Villen, J. (2013). Global analysis of phosphorylation and ubiquitylation cross-talk in protein degradation. Nat. Methods *10*, 676–682.

Tachibana, M., Sugimoto, K., Fukushima, T., and Shinkai, Y. (2001). Set domain-containing protein, G9a, is a novel lysine-preferring mammalian histone methyltransferase with hyperactivity and specific selectivity to lysines 9 and 27 of histone H3. J. Biol. Chem. *276*, 25309–25317.

Tadokoro, Y., Ema, H., Okano, M., Li, E., and Nakauchi, H. (2007). De novo DNA methyltransferase is essential for self-renewal, but not for differentiation, in hematopoietic stem cells. J. Exp. Med. *204*, 715–722.

Tahiliani, M., Koh, K.P., Shen, Y., Pastor, W.A., Bandukwala, H., Brudno, Y., Agarwal, S., Iyer, L.M., Liu, D.R., Aravind, L., et al. (2009). Conversion of 5-methylcytosine to 5-hydroxymethylcytosine in mammalian DNA by MLL partner TET1. Science *324*, 930–935.

Tsumura, A., Hayakawa, T., Kumaki, Y., Takebayashi, S., Sakaue, M., Matsuoka, C., Shimotohno, K., Ishikawa, F., Li, E., Ueda, H.R., et al. (2006). Maintenance of self-renewal ability of mouse embryonic stem cells in the absence of DNA methyltransferases Dnmt1, Dnmt3a and Dnmt3b. Genes Cells *11*, 805–814.

Vincent, J.J., Huang, Y., Chen, P.Y., Feng, S., Calvopina, J.H., Nee, K., Lee, S.A., Le, T., Yoon, A.J., Faull, K., et al. (2013). Stage-specific roles for tet1 and tet2 in DNA demethylation in primordial germ cells. Cell Stem Cell *12*, 470–478.

von Meyenn, F., Iurlaro, M., Habibi, E., Liu, N.Q., Salehzadeh-Yazdi, A., Santos, F., Petrini, E., Milagre, I., Yu, M., Xie, Z., et al. (2016). Impairment of DNA methylation maintenance is the main cause of global demethylation in naive embryonic stem cells. Mol. Cell *62*, 848–861.

Wang, J., Zhang, M., Zhang, Y., Kou, Z., Han, Z., Chen, D.Y., Sun, Q.Y., and Gao, S. (2010). The histone demethylase JMJD2C is stage-specifically expressed in preimplantation mouse embryos and is required for embryonic development. Biol. Reprod. *82*, 105–111.

Whetstine, J.R., Nottke, A., Lan, F., Huarte, M., Smolikov, S., Chen, Z., Spooner, E., Li, E., Zhang, G., Colaiacovo, M., et al. (2006). Reversal of histone lysine trimethylation by the JMJD2 family of histone demethylases. Cell *125*, 467–481.

Williams, R.L., Hilton, D.J., Pease, S., Willson, T.A., Stewart, C.L., Gearing, D.P., Wagner, E.F., Metcalf, D., Nicola, N.A., and Gough, N.M. (1988). Myeloid leukaemia inhibitory factor maintains the developmental potential of embryonic stem cells. Nature *336*, 684–687.

Wray, J., and Hartmann, C. (2012). WNTing embryonic stem cells. Trends Cell Biol. *22*, 159–168.

Wu, H., Chen, X., Xiong, J., Li, Y., Li, H., Ding, X., Liu, S., Chen, S., Gao, S., and Zhu, B. (2011). Histone methyltransferase G9a contributes to H3K27 methylation in vivo. Cell Res. *21*, 365–367.

Yamaji, M., Seki, Y., Kurimoto, K., Yabuta, Y., Yuasa, M., Shigeta, M., Yamanaka, K., Ohinata, Y., and Saitou, M. (2008). Critical function of Prdm14 for the establishment of the germ cell lineage in mice. Nat. Genet. *40*, 1016–1022.

Yamaji, M., Ueda, J., Hayashi, K., Ohta, H., Yabuta, Y., Kurimoto, K., Nakato, R., Yamada, Y., Shirahige, K., and Saitou, M. (2013). PRDM14 ensures naive pluripotency through dual regulation of signaling and epigenetic pathways in mouse embryonic stem cells. Cell Stem Cell *12*, 368–382.

Ying, Q.L., Wray, J., Nichols, J., Batlle-Morera, L., Doble, B., Woodgett, J., Cohen, P., and Smith, A. (2008). The ground state of embryonic stem cell self-renewal. Nature *453*, 519–523.

Yu, C., Zhang, Y.L., Pan, W.W., Li, X.M., Wang, Z.W., Ge, Z.J., Zhou, J.J., Cang, Y., Tong, C., Sun, Q.Y., et al. (2013). CRL4 complex regulates mammalian oocyte survival and reprogramming by activation of TET proteins. Science *342*, 1518–1521.

Zhang, X., Peterson, K.A., Liu, X.S., McMahon, A.P., and Ohba, S. (2013). Gene regulatory networks mediating canonical Wnt signal-directed control of pluripotency and differentiation in embryo stem cells. Stem Cells *31*, 2667–2679.

Stem Cell Reports, Volume *8*

Supplemental Information

2i Maintains a Naive Ground State in ESCs through Two Distinct Epigenetic Mechanisms

Ye-Ji Sim, Min-Seong Kim, Abeer Nayfeh, Ye-Jin Yun, Su-Jin Kim, Kyung-Tae Park, Chang-Hoon Kim, and Kye-Seong Kim

Supplemental information

Supplemental Materials and Methods

Cell culture and inhibitors

The mouse ESC lines J1 (ATCC SCRC-1010), CCE, and *Jmjd2c* KO were cultured on mitomycin C-treated CF1 MEF feeder cells or 0.1% gelatin-coated plates at 37°C with 5% CO_2 in Dulbecco's modified Eagle medium (DMEM; Hyclone) supplemented with 15% fetal bovine serum (FBS; Hyclone), 0.1 mM β-mercaptoethanol (Gibco), 100× penicillin/streptomycin (Gibco), 2 mM GlutaMAX (Gibco), 0.1 mM NEAA, and 1000 U/ml LIF (Millipore). We passaged the ESCs at a ratio of 1:20 every 3 days. We cultured 293T cells in DMEM supplemented with 10% FBS, 100× penicillin/streptomycin (Gibco), 2 mM GlutaMAX (Gibco), and 0.1 mM NEAA at 37°C with 5% CO_2. For the 2i culture condition, we cultured ESCs on 0.1% coated gelatin plates using the same ESC culture medium supplemented with Mek1 and Gsk3 inhibitors without LIF. We used the following inhibitors in our study: 1 μM PD0325901 (Stemgent, 04-0006-02), 3 μM CHIR99021 (Stemgent, 04-0004-02), 5 μM FR180204 (Millipore, 328010), 10 μM SU5402 (Abmole, M2194), 5 μM MG132 (Merck, 474790), 5 μM 5-Carboxyl-8-HQ (Merck, 420201), and 1–10 μM UNC0638 (Sigma-Aldrich, U4885).

Dot blot

We isolated genomic DNA (gDNA) using the Qiagen DNeasy Blood & Tissue Kit according to the manufacturer's protocol. We denatured the isolated gDNA in 0.8 M NaOH/20 mM EDTA for 10 min at 95°C. We then neutralized the samples with 2 M ammonium acetate (pH7.0) and serially diluted them twofold. We spotted the samples on a nitrocellulose membrane using a Bio-Dot apparatus (Bio-Rad). We washed the blotted membrane in 2×SSC buffer and exposed it to UV light for 2 min. After blocking the membrane with 5% skim milk for 1 hour, we incubated it overnight at 4°C with primary antibodies diluted in blocking solution. The primary antibodies were mouse anti-5-methylcytosine antibody (Abcam 1:500) and rabbit anti-5-hydroxymethylcytosine polyclonal antibody (Active Motif, 1:2000).

Quantitative reverse transcription-polymerase chain reaction (qRT-PCR)

We extracted total RNA with TRIzol reagent (Invitrogen) according to the manufacturer's protocol. We dissolved the RNA pellets in nuclease-free water and determined the RNA concentration of each sample with a NanoDrop. We reverse-transcribed 1 μg RNA into cDNA using SuperScript III Reverse Transcriptase (Invitrogen). We amplified the cDNA using IQ

SYBR Green Supermix (Bio-Rad) with appropriate PCR primer sets (Table S2). We performed real-time PCR assays on a CFX96 Touch real-time PCR detection system.

Table S2. qPCR primers used in the study

	Forward	**Reverse**
L32	CGCAAGTTCCTGGTCCACA	TGCTGCTCTTTCTACAATGGCT
Jmjd2c	ATGGATCGCAGATTGCAATGA	TTCCTCTCCCCTTGGATTACAT
Oct4	TAGCATTGAGAACCGTGTGAG	ACTTGATCTTTTGCCCTTCTGG
Sox2	TTTGCAAGCAACTTTTGTACAGTA	TCCTTCCTTGTTTGTAACGGTC
Dnmt3a	CCATTACCACCAGGTCAAACTCTA	AAGCGGCTCATGTTGGAGAC
Dnmt3b	ACAACCGTCCATTCTTCTGGAT	TTCATTCCGGGTAGGTTACC
Dnmt3l	AGGATGTCCGTGGCAGAGACTA	AGCTTGCTCCTGCTTCTGACTT
Tet1	CTTTCTCTGGTGTCACCTGTTG	TATAGTGGCAGGACGTGGAGTT
Tet2	ATTCTCAGGAGTCACTGCATGTT	TACATAGGCAGCACGTGGAACT
Prdm14	TTCTTCACGTCCATGAGAGGC	TCTGATGTGTGTTCGGAGTATGCT
G9a	AAGATCTACGGTTCCCACGCATT	TTGCACTTCTCAGAGCCACACT

Generation of mouse *Jmjd2c* KO ESCs

We transfected cells with pSpCas9(BB)-2A-GFP (PX458) or pSpCas9(BB)-2A-Puro (PX459) (Addgene #48138, 48139) to clone a *Jmjd2c*-guide sequence. We performed an insert/deletion assay using T7 endonuclease I (NEB). To generate *Jmjd2c* KO ESCs, we transfected CCE cells with pSpCas9 (BB) containing *Jmjd2c*-guide RNA and homologous recombination (HR) donor with a puromycin selection cassette. We incubated the cells with 3 μg/ml puromycin to isolate puromycin-resistant colonies. We confirmed HR events by gDNA-mediated PCR to detect HR events in selected colonies. Finally, we confirmed the *Jmjd2c* KO cells by PCR, sequencing, and Western blot.

Western blot

To perform Western blot analysis, we washed the cells with PBS and lysed them with RIPA buffer (50 mM Tris-HCl pH 7.4, 150 mM of NaCl, 1% sodium deoxycholate, 1% Triton X-100, and 0.1% SDS). We used the cell lysates for Western blots and other experiments. We subjected 20 μg lysate protein to SDS-polyacrylamide gel electrophoresis, transferred it to a PVDF membrane, and blotted it with appropriate antibodies. We detected proteins using HRP-conjugated secondary antibodies and ECL reagents. We visualized the bands using the ChemiDoc MP System (Bio-Rad).

GST pull down, *in vitro* kinase assay, ubiquitination assay, and *in vitro* methylation assay

For the pull-down analysis, we generated a mammalian GST expression vector system. We transfected GST-transgenes into 293T cells using a PEI transfection method. Two days after transfection, we washed cells with PBS and lysed them with RIPA buffer (50 mM Tris-HCl pH 7.4, 150 mM NaCl, 1% sodium deoxycholate, 1% Triton X-100, and 0.1% SDS). After clarifying cell lysates in a microcentrifuge, we added Glutathione Sepharose 4B and incubated them at 4°C overnight. We then washed the beads with RIPA buffer three times, added 1×SDS sample buffer, and performed Western blots.

We conducted an *in vitro* Mek1 kinase assay as follows. We transfected GST-JMJD2C and GST-MEK1 into 293T cells, isolated the proteins individually using glutathione beads, mixed them together, and incubated them in kinase buffer (25 mM Tris-HCl pH 7.5, 150 mM NaCl, 10 mM $MgCl_2$, 20 mM β-GP, 100 μM Na_3O_4V, 400 μM ATP, and 2 mM DTT) for 6 h at 37°C. We stopped the reaction by adding 2×SDS sample buffer and then performed Western blots. For ubiquitination assays, we transfected GST-JMJD2C and 5Myc-MEK1 with HA-Ub separately into 293T cells. We detected JMJD2C ubiquitination using anti-HA antibody after the pull-down assay. After washing the beads three times with RIPA buffer, we added 1×SDS sample buffer and performed Western blots.

We transfected GST-PRDM14, GST-DNMT1, GST-DNMT3A, and/or DNMT3B into 293T cells, individually isolated the proteins using glutathione beads, mixed them together, and incubated them in methylation buffer (50 mM Tris-HCl pH 8.8, 5 mM $MgCl_2$, and 4 mM DTT) with S-adenosyl-l-[methyl-^{3}H] methionine (85 Ci/mmol from a 0.5 mCi/ml stock solution, Perkin-Elmer) for 6 hours at RT. We stopped the reaction by adding 2×SDS sample buffer and performed Western blots. We used the following antibodies: anti-JMJD2C (Abcam, ab85454 or Bethyl, A300-885A), anti-GAPDH (Cell signaling, 2118), anti-H3K4me3 (Millipore, 07-473), anti-H3K4me2 (Millipore, 07-030), anti-H3K9me3 (Abcam, ab8898), anti-H3K9me2 (Abcam, ab1220), anti-H3K27me3 (Millipore, 07-449), anti-H3K27me2 (Millipore, 07-451), anti-H3K36me3 (Abcam, ab9050), anti-H3K36me2 (Millipore, 07-369), anti-Histone3 (Abcam, ab1791), anti-OCT4 (Santa, sc-5279), anti-SOX2 (Abcam, ab97959), anti-Phospho-ERK1/2 (Cell Signaling, 9106), anti-ERK1/2 (Cell Signaling 9102), anti-4G10 (Millipore, 05-321), anti-GST (Abfrontier, LF-PA0189), anti-HA (Santa, sc-7392), anti-Myc (Santa, sc-40), anti-GFP (Santa, sc-9996), anti-DNMT3A (Novus, IMG-268A), anti-DNMT3B (Abcam, ab2851), anti-FLAG (Sigma, F3165), anti-TET1 (Abcam, ab156993), and anti-PRDM14 (Abcam, ab187881).

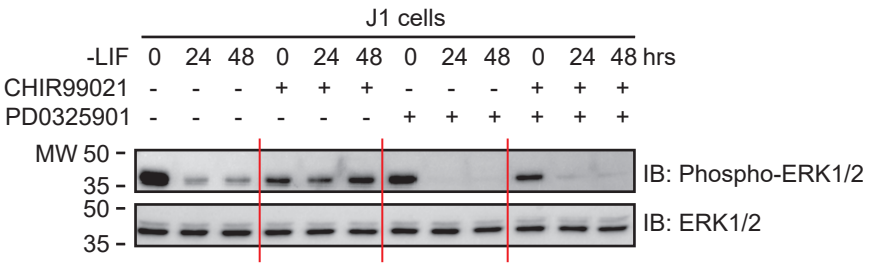
J1 cells
-LIF 0 24 48 0 24 48 0 24 48 0 24 48 hrs
CHIR99021 - - - + + + - - - + + +
PD0325901 - - - - - - + + + + + +
MW 50
35
50
35
IB: Phospho-ERK1/2
IB: ERK1/2

Figure S1

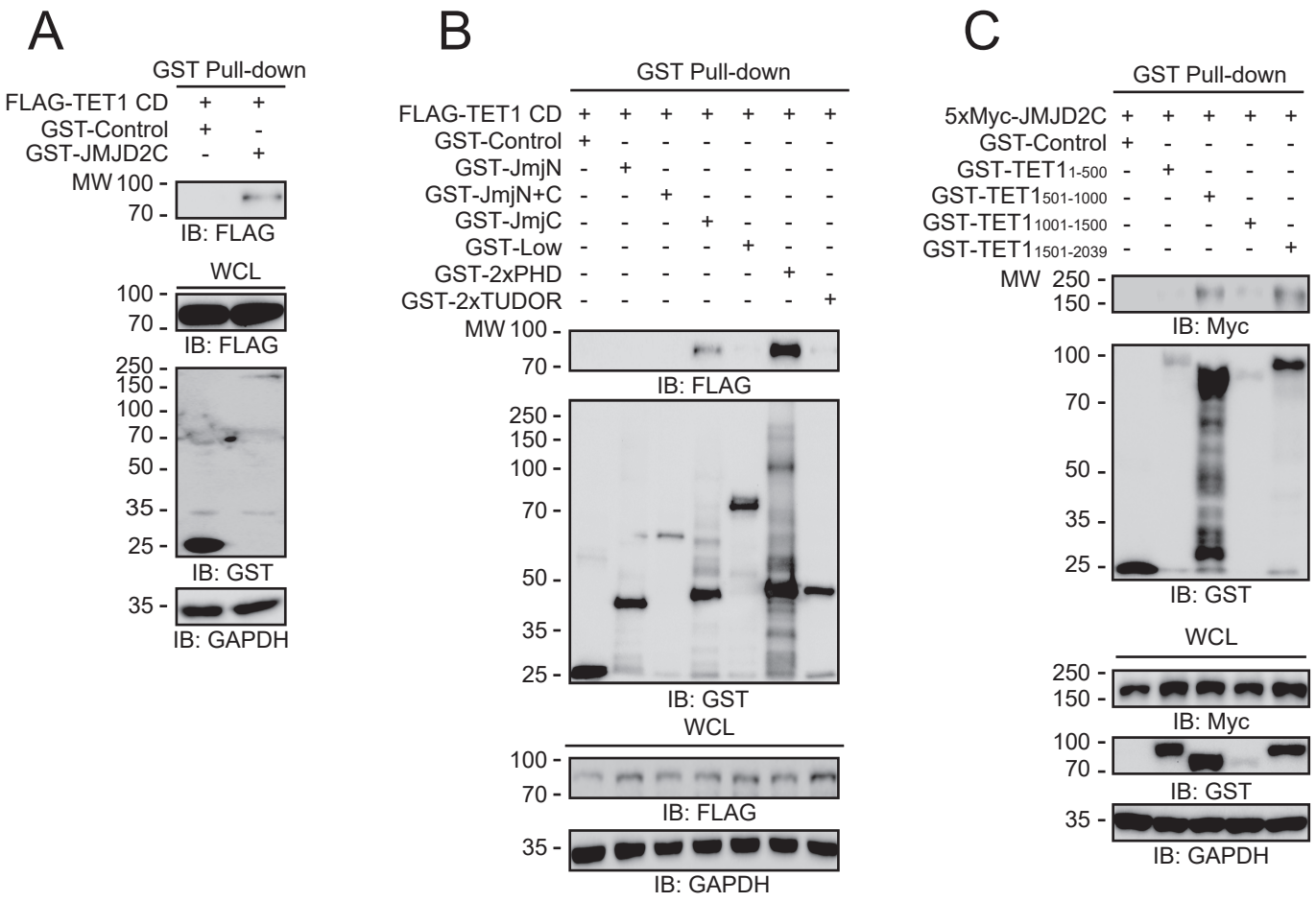
A
GST Pull-down
FLAG-TET1 CD + +
GST-Control + -
GST-JMJD2C - +
MW 100 -
70 -
IB: FLAG
WCL
100 -
70 -
IB: FLAG
250 -
150 -
100 -
70 -
50 -
35 -
25 -
IB: GST
35 -
IB: GAPDH
B
GST Pull-down
FLAG-TET1 CD + + + + + + +
GST-Control + - - - - - -
GST-JmjN - + - - - - -
GST-JmjN+C - - + - - - -
GST-JmjC - - - + - - -
GST-Low - - - - + - -
GST-2xPHD - - - - - + -
GST-2xTUDOR - - - - - - +
MW 100 -
70 -
IB: FLAG
250 -
150 -
100 -
70 -
50 -
35 -
25 -
IB: GST
WCL
100 -
70 -
IB: FLAG
35 -
IB: GAPDH
C
GST Pull-down
5xMyc-JMJD2C + + + + +
GST-Control + - - - -
GST-TET1 1-500 - + - - -
GST-TET1 501-1000 - - + - -
GST-TET1 1001-1500 - - - + -
GST-TET1 1501-2039 - - - - +
MW 250 -
150 -
IB: Myc
100 -
70 -
50 -
35 -
25 -
IB: GST
WCL
250 -
150 -
IB: Myc
100 -
70 -
IB: GST
35 -
IB: GAPDH

Figure S2

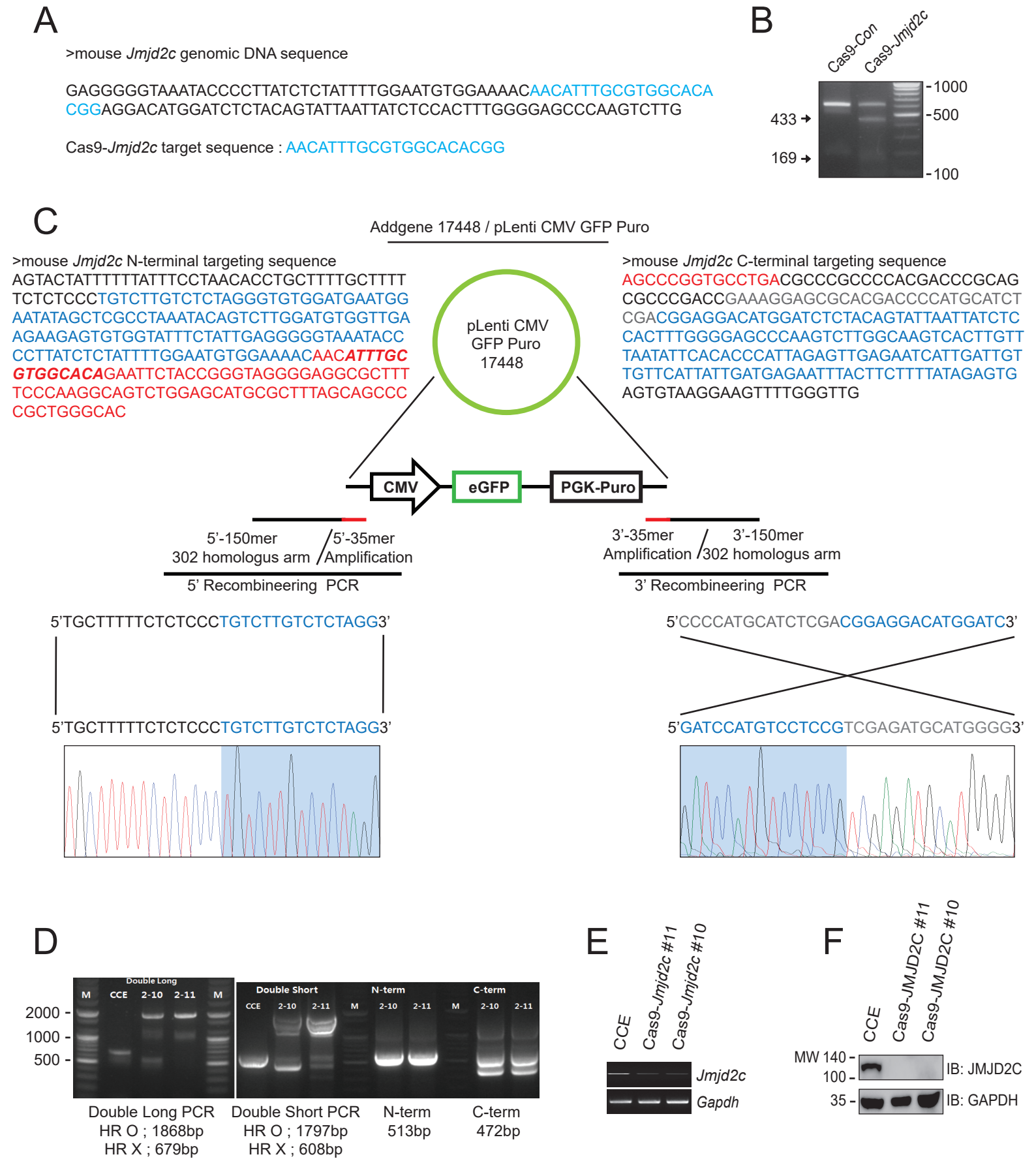
A
>mouse Jmjd2c genomic DNA sequence
GAGGGGGTAAATACCCCTTATCTCTATTTTGGAATGTGGAAAACAACATTTGCGTGGCACA
CGGAGGACATGGATCTCTACAGTATTAATTATCTCCACTTTGGGGAGCCCAAGTCTTG
Cas9-Jmjd2c target sequence : AACATTTGCGTGGCACACGG
B
Cas9-Con
Cas9-Jmjd2c
433
169
1000
500
100
C
Addgene 17448 / pLenti CMV GFP Puro
>mouse Jmjd2c N-terminal targeting sequence
AGTACTATTTTTTATTTCCTAACACCTGCTTTTGCTTTT
TCTCTCCCTGTCTTGTCTCTAGGGTGTGGATGAATGG
AATATAGCTCGCCTAAATACAGTCTTGGATGTGGTTGA
AGAAGAGTGTGGTATTTCTATTGAGGGGGTAAATACC
CCTTATCTCTATTTTGGAATGTGGAAAACAAC***ATTTGC***
GTGGCACAGAATTCTACCGGGTAGGGGAGGCGCTTT
TCCCAAGGCAGTCTGGAGCATGCGCTTTAGCAGCCC
CGCTGGGCAC
>mouse Jmjd2c C-terminal targeting sequence
AGCCCGGTGCCTGACGCCCGCCCCACGACCCGCAG
CGCCCGACCGAAAGGAGCGCACGACCCCATGCATCT
CGACGGAGGACATGGATCTCTACAGTATTAATTATCTC
CACTTTGGGGAGCCCAAGTCTTGGCAAGTCACTTGTT
TAATATTCACACCCATTAGAGTTGAGAATCATTGATTGT
TGTTCATTATTGATGAGAATTTACTTCTTTTATAGAGTG
AGTGTAAGGAAGTTTTGGGTTG
pLenti CMV GFP Puro 17448
CMV
eGFP
PGK-Puro
5'-150mer 302 homologus arm
5'-35mer Amplification
5' Recombineering PCR
3'-35mer Amplification
3'-150mer 302 homologus arm
3' Recombineering PCR
5'TGCTTTTTCTCTCCCTGTCTTGTCTCTAGG3'
5'TGCTTTTTCTCTCCCTGTCTTGTCTCTAGG3'
5'CCCCATGCATCTCGACGGAGGACATGGATC3'
5'GATCCATGTCCTCCGTCGAGATGCATGGGG3'
D
Double Long
M
CCE
2-10
2-11
M
Double Short
N-term
C-term
CCE
2-10
2-11
M
2-10
2-11
M
2-10
2-11
2000
1000
500
Double Long PCR
HR O ; 1868bp
HR X ; 679bp
Double Short PCR
HR O ; 1797bp
HR X ; 608bp
N-term
513bp
C-term
472bp
E
CCE
Cas9-Jmjd2c #11
Cas9-Jmjd2c #10
Jmjd2c
Gapdh
F
CCE
Cas9-JMJD2C #11
Cas9-JMJD2C #10
MW 140
100
35
IB: JMJD2C
IB: GAPDH

Figure S3

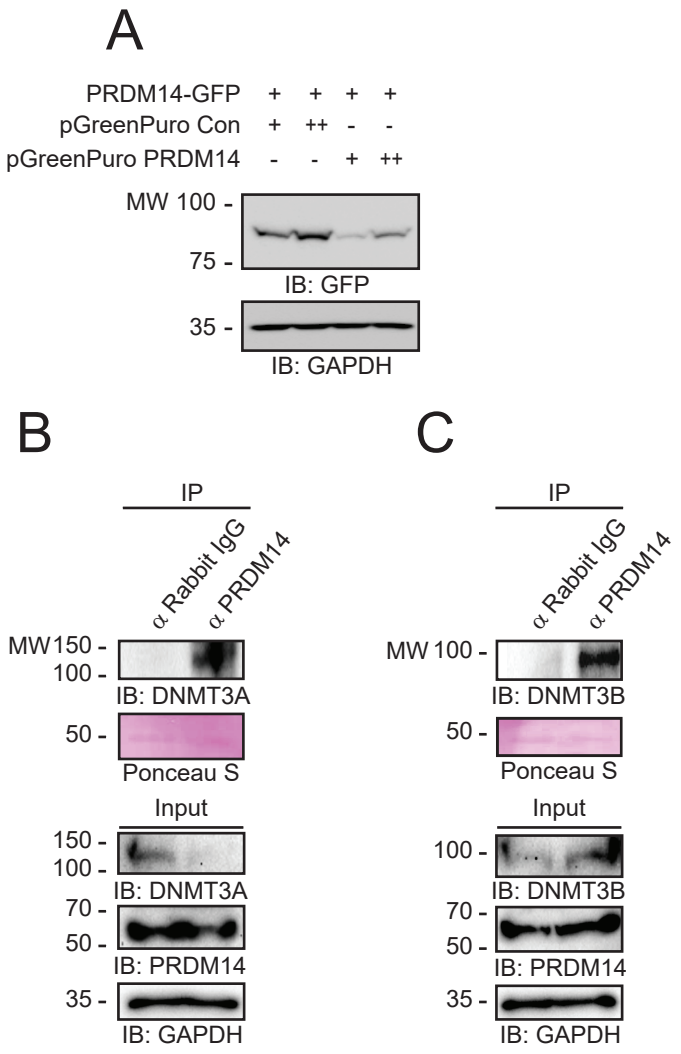
A
PRDM14-GFP + + + +
pGreenPuro Con + ++ - -
pGreenPuro PRDM14 - - + ++
MW 100 -
75 -
IB: GFP
35 -
IB: GAPDH
B
IP
α Rabbit IgG
α PRDM14
MW150 -
100 -
IB: DNMT3A
50 -
Ponceau S
Input
150 -
100 -
IB: DNMT3A
70 -
50 -
IB: PRDM14
35 -
IB: GAPDH
C
IP
α Rabbit IgG
α PRDM14
MW 100 -
IB: DNMT3B
50 -
Ponceau S
Input
100 -
IB: DNMT3B
70 -
50 -
IB: PRDM14
35 -
IB: GAPDH

Figure S4

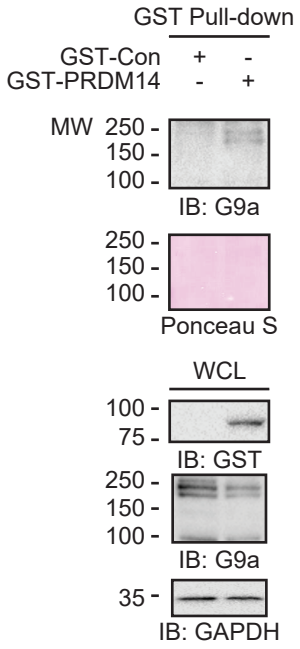
GST Pull-down
GST-Con + -
GST-PRDM14 - +
MW 250 -
150 -
100 -
IB: G9a
250 -
150 -
100 -
Ponceau S
WCL
100 -
75 -
IB: GST
250 -
150 -
100 -
IB: G9a
35 -
IB: GAPDH

Figure S5

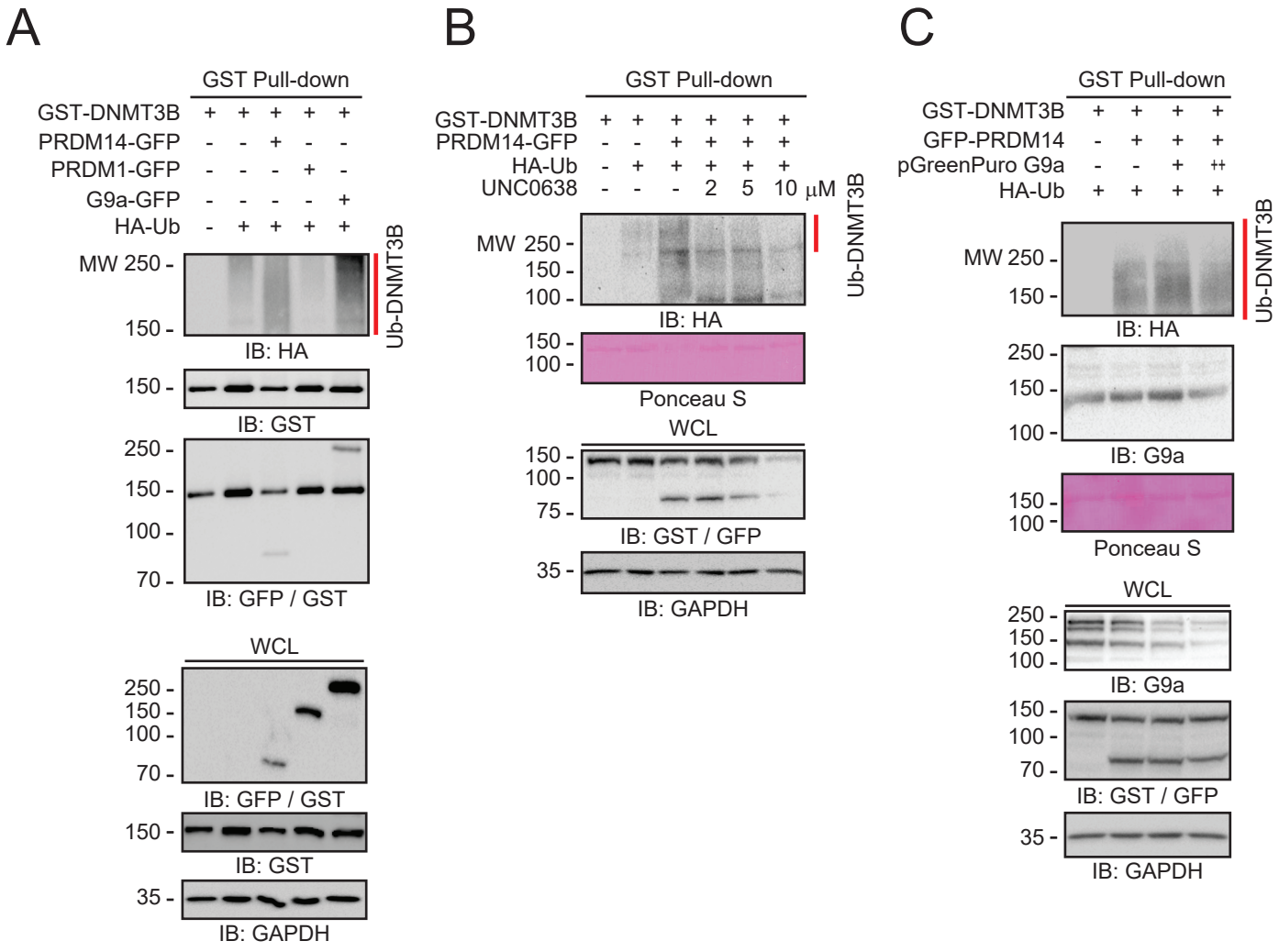
A
GST Pull-down
GST-DNMT3B + + + + +
PRDM14-GFP - - + - -
PRDM1-GFP - - - + -
G9a-GFP - - - - +
HA-Ub - + + + +
MW 250 -
150 -
Ub-DNMT3B
IB: HA
150 -
IB: GST
250 -
150 -
100 -
70 -
IB: GFP / GST
WCL
250 -
150 -
100 -
70 -
IB: GFP / GST
150 -
IB: GST
35 -
IB: GAPDH
B
GST Pull-down
GST-DNMT3B + + + + + +
PRDM14-GFP - - + + + +
HA-Ub - + + + + +
UNC0638 - - - 2 5 10 μM
MW 250 -
150 -
100 -
Ub-DNMT3B
IB: HA
150 -
100 -
Ponceau S
WCL
150 -
100 -
75 -
IB: GST / GFP
35 -
IB: GAPDH
C
GST Pull-down
GST-DNMT3B + + + +
GFP-PRDM14 - + + +
pGreenPuro G9a - - + ++
HA-Ub + + + +
MW 250 -
150 -
Ub-DNMT3B
IB: HA
250 -
150 -
100 -
IB: G9a
150 -
100 -
Ponceau S
WCL
250 -
150 -
100 -
IB: G9a
150 -
100 -
70 -
IB: GST / GFP
35 -
IB: GAPDH

Figure S6

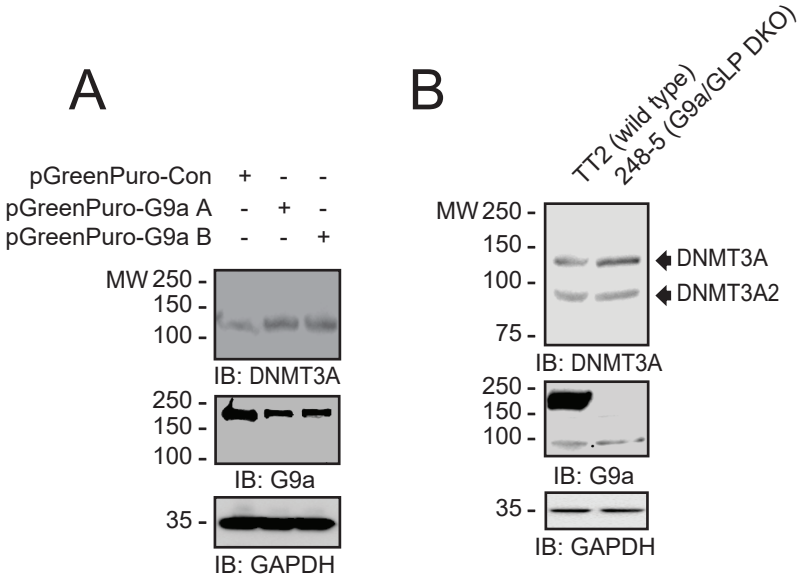
A
pGreenPuro-Con + - -
pGreenPuro-G9a A - + -
pGreenPuro-G9a B - - +
MW 250 -
150 -
100 -
IB: DNMT3A
250 -
150 -
100 -
IB: G9a
35 -
IB: GAPDH
B
TT2 (wild type)
248-5 (G9a/GLP DKO)
MW 250 -
150 -
100 -
75 -
DNMT3A
DNMT3A2
IB: DNMT3A
250 -
150 -
100 -
IB: G9a
35 -
IB: GAPDH

Figure S7

Supplemental figure legends

Figure S1 (related to Figure 1)

PD0325901, but not CHIR99021, specifically decreases phospho-ERK1/2 levels.

Figure S2 (related to Figure 3)

TET1 associates with JMJD2C.

(A) A pull-down assay shows that TET1 CD, a TET1 catalytic mutant, associates with JMJD2C. (B) A pull-down assay shows that TET1 CD binds to the JmjC and 2×PHD domains in JMJD2C. (C) A pull-down assay shows that JMJD2C associates with the CXXC and CD domains of TET1.

Figure S3 (related to Figure 3)

***Jmjd2c* KO strategy using CRISPR/Cas9 technology.**

(A) Mouse *Jmjd2c* genomic DNA sequences and a *Jmjd2c*-specific 20-bp guide RNA sequence. (B) T7 Endonuclease I assay shows that a *Jmjd2c*-specific guide RNA effectively targets *Jmjd2c* genomic DNA. (C) To disrupt genomic regions of the *Jmjd2c* gene through homologous recombination with an antibiotic puromycin cassette, we designed the primers containing the gene-specific homologous sequences (150 bp) with amplifying gene sequences (30 bp) for the PGK-Puro cassette using pLenti GFP Puro (Addgene Plasmid #17448) as a template. (D) Puromycin-resistant ESC colonies are determined by increasing PCR size due to the insertion of HR donor into *Jmjd2c* genomic DNA. To identify HR donor insertion by homologous recombination, 5’ and 3’ gene-specific primers were chosen from the adjacent upstream and downstream regions of the HR destination site in *Jmjd2c*. (E) *Jmjd2c*-KO clones have reduced *Jmjd2c* mRNA levels compared with control CCE cells, determined using RT-PCR assay. (F) *Jmjd2c*-KO clones do not express JMJD2C proteins as revealed by a Western blot.

Figure S4 (related to Figure 4)

PRDM14 associates with DNMT3A and DNMT3B.

(A) pGreenPuro *Prdm14*, a *Prdm14* shRNA, decreases PRDM14 expression

(B) Endogenous PRDM14 binds to DNMT3A in an immunoprecipitation assay. (C) Endogenous DNMT3B associates with PRMD14 in an immunoprecipitation assay.

Figure S5 (related to Figure 5)

GST-PRDM14 associates with endogenous G9a in a pull-down assay.

Figure S6 (related to Figure 5)

PRDM14-mediated G9a promotes DNMT3B ubiquitination.

(A) DNMT3B ubiquitination is increased in proportion to the expression of G9a > PRDM14 > Control > PRDM1 in a GST pull-down assay. (B) A GST pull-down assay shows that DNMT3B ubiquitination is increased by PRDM14, whereas UNC0638 inhibits a PRDM14-mediated DNMT3B degradation in a dose-dependent manner. (C) Silencing of endogenous *G9a* using pGreenPuro *G9a* reduces DNMT3B ubiquitination.

Figure S7 (related to Figure 7)

G9a/GLP deficiency causes an increase of DNMT3A protein levels.

(A) Western blots show that knockdown of G9a expression by pGreenPuro *G9a-A* and *-B* increases endogenous DNMT3A expression. (B) Western blots reveal that deficiency of *G9a* and *GLP* increases DNMT3A protein levels in the 248-5 ESC cell line compared with wild-type TT2 cells.

Supplemental Table S1

		DEGs (fold-change threshold: 99% of null)				P-value				log2-fold-change																				
Gene ID	Gene Symbol	2iLIF/DMSO	2i/DMSO	CHIR/DMSO	PD/DMSO	2iLIF/DMSO	2i/DMSO	CHIR/DMSO	PD/DMSO	2iLIF/DMSO	2i/DMSO	CHIR/DMSO	PD/DMSO	GSM1062296 2iLIF_1	GSM1062297 2iLIF_2	GSM1062298 2iLIF_3	GSM1062299 2i_1	GSM1062300 2i_2	GSM1062301 2i_3	GSM1062302 CHIR_1	GSM1062303 CHIR_2	GSM1062304 CHIR_3	GSM1062305 PD03_1	GSM1062306 PD03_2	GSM1062307 PD03_3	GSM1062308 DMSO_1	GSM1062309 DMSO_2	GSM1062310 DMSO_3
NM_001081209	Prdm14	up	up	up	up	2.08E-05	1.78E-05	4.43E-05	1.82E-06	2.6937435	2.34664416	1.390618992	1.936412179	9.734662919	9.759732764	9.728707596	9.240583411	9.387563579	9.448215371	8.36141719	8.431538411	8.514229286	8.964565943	8.977331598	8.977331598	7.040919419	7.113215776	7.020838302
NM_007548	Prdm1	up	up	--	up	0.015374885	0.018305151	0.889130277	0.000498108	0.581183883	0.421455258	0.02536966	0.885518698	7.676576678	7.750157138	7.809001314	7.590428513	7.677852968	7.499011318	7.089715969	7.194342915	7.237305238	8.110252936	7.956157	8.054491953	7.312161899	7.168973265	7.112545712
NM_011535	Tbx3	up	up	up	up	0.000188878	0.000122543	0.000238796	0.001625501	2.581117932	1.923297366	1.355536961	0.84483231	10.40761161	10.32354924	10.2811795	9.640098166	9.722249172	9.665718674	9.062702788	9.172724328	9.097968269	8.480920935	8.621280203	8.587263618	8.008584586	7.626197293	7.742431308
NM_177099	Lefty2	up	up	up	up	5.30E-06	5.17E-07	8.61E-06	6.53E-07	4.31458919	3.934158218	1.993614377	2.859179016	9.894282973	9.925499612	9.768624961	9.363892349	9.513852001	9.643134575	7.57330816	7.47760483	7.633268096	8.438872799	8.387664087	8.551826999	5.478257139	5.579693783	5.619299399
NM_010094	Lefty1	up	up	up	up	0.000169583	3.07E-06	0.000177938	8.30E-07	3.175251135	3.96176601	1.839246142	3.78969569	9.628162157	9.745735212	9.690076275	10.39588146	10.47659115	10.54332629	8.298337367	8.354071282	8.425055434	10.21191	10.30452083	10.40687749	5.967479632	6.744165359	6.51482514
NM_026796	Smyd2	up	up	up	up	0.001394222	0.000458713	0.000641199	0.001161743	1.494694834	1.438612042	1.004273727	0.801399211	9.30780558	9.46350715	9.389697544	9.160576543	9.333614752	9.352680818	8.81566046	8.911742177	8.899276437	8.736603081	8.656722313	8.696401921	7.89500271	7.808687401	8.114987414
NM_013611	Nodal	up	up	up	up	0.000367443	4.67E-05	1.70E-05	2.44E-05	1.529936354	1.615492264	1.257028321	1.12330889	10.26603101	10.36085282	10.23243931	10.35158692	10.24952867	10.35496544	9.983344185	9.993122977	10.01512809	9.850712405	9.859403546	9.907517928	8.736094656	8.75469834	8.687766487
NM_008816	Pecam1	up	up	up	up	0.010766991	0.004162959	0.008929888	0.008131249	0.853203199	0.791584336	0.568051215	0.529394893	9.617938224	9.749584955	9.720535044	9.648232494	9.700653777	9.668916181	9.350158745	9.491353159	9.43538306	9.396726738	9.375189418	9.458740539	9.154002822	8.867331845	8.823570533
NM_001159500	Esrrb	up	up	up	up	0.003316319	0.001722777	0.00342007	0.002628875	1.19294666	1.00258396	0.69134219	0.70113917	11.66703712	11.70981212	11.6542869	11.47471628	11.47665442	11.51315757	11.16541265	11.16100748	11.21460694	11.17969821	11.1709077	11.17520963	10.73581495	10.47407046	10.38108872
NM_008235	Hes1	up	up	up	up	0.000243889	0.000172928	0.00122072	0.002357167	1.828768241	1.220376893	0.726373658	0.742781808	9.377064875	9.310411597	9.248213301	8.752585227	8.681640153	8.702002249	8.208017014	8.329053562	8.115068294	8.292115473	7.951240993	8.224425164	7.553524088	7.481643356	7.423561014
NM_009694	Apobec2	up	up	up	up	0.00073187	0.000230407	0.00100059	0.000142323	1.897923915	1.691566139	0.639195488	1.384445177	9.595004172	9.663694771	9.784248094	9.457336995	9.375916202	9.464262913	8.205240129	8.579430112	8.404966344	9.135297842	9.203014836	9.150216033	8.055604884	7.703379932	7.765770856
NM_008452	Klf2	up	up	up	up	0.000386747	0.000109329	9.27E-05	2.92E-05	1.38690784	1.31390931	0.988623174	1.21855983	10.12457281	10.08904652	10.0939834	10.02098487	10.00554933	10.08050307	9.695698734	9.674610688	9.704146094	9.92563539	9.956417994	9.898291188	8.791942629	8.70707556	8.690499
NM_010637	Klf4	up	up	up	up	0.000140419	0.000427339	0.000297603	0.007711892	2.685471163	1.304755636	1.163306683	0.544261596	10.06780809	9.853522256	9.819504993	8.422381824	8.472836729	8.510343403	8.393148032	8.331441776	8.243525405	7.946282585	7.570614741	7.712342689	7.266383853	6.971213521	7.168081093
NM_173780	Klf8	up	up	up	up	0.001833927	0.001262853	0.002995577	0.000918119	1.443620126	1.127134742	0.743156225	0.947144003	10.22436429	10.23641037	10.17911043	9.861520042	9.907878906	9.973130342	9.468154669	9.523900389	9.544040012	9.727888167	9.637016966	9.754951787	9.055430513	8.692796398	8.780744164
NM_028016	Nanog	up	up	up	up	0.002646581	0.000709352	0.000874425	0.000378383	1.00864412	0.97985524	0.73748891	0.85312098	12.71561246	12.76219024	12.67611748	12.66457041	12.68682358	12.71849913	12.42537538	12.44445725	12.44945098	12.56008932	12.53749764	12.5954956	11.85690756	11.70696834	11.66723663
NM_001038695	Kdm3a	up	up	up	up	0.002362949	0.00039174	0.000585021	0.000244472	0.72941103	0.62571509	0.55650105	0.59326283	11.15419626	11.24088232	11.16668202	11.09236587	11.06288608	11.09263587	10.94699935	11.03953382	10.99377204	11.03053382	10.9813431	11.03821171	10.44660054	10.41496279	10.43727099
NM_011567	Tead4	up	up	up	up	0.00096028	0.00025724	0.000809718	0.002993825	1.255557287	0.880686081	0.525141108	0.398197823	10.33780188	10.37898115	10.22344488	9.934756294	9.962930674	9.971883822	9.653896468	9.607385701	9.590313758	9.480442416	9.59507105	9.480202752	9.099589833	9.026808214	9.082244593
NM_001166584	Tead1	up	up	up	up	0.012334144	0.003018747	0.004875627	0.003787883	0.612960083	0.684819563	0.544222183	0.500647833	10.33239521	10.40377108	10.32981643	10.40425469	10.42212806	10.38425853	10.35477357	10.26365731	10.18181986	10.22008296	10.25664611	10.19310094	9.884421547	9.673273905	9.719435127
NM_001122733	Kit	up	up	up	up	0.000565536	0.000510548	0.002016518	0.006722219	2.127678311	1.550875491	0.92702609	0.652810213	10.63535073	10.70207044	10.62866825	10.05854791	10.11315151	10.01755924	9.434698509	9.530332563	9.396293103	9.147440186	9.303593616	9.160482632	8.897316678	8.507672419	8.472143779
NM_013633	Pou5f1	--	--	--	--	0.752532776	0.554494344	0.444950151	0.66441425	-0.03193208	-0.03193208	-0.04637732	-0.01963887	12.55592081	12.51253421	12.47263575	12.51253421	12.4720509	12.52785514	12.49808897	12.44931726	12.53041096	12.5339524	12.50332011	12.52482742	12.52332201	12.54446629	12.56011014
NM_011443	Sox2	--	--	--	--	0.230457536	0.255813153	0.323908414	0.066274529	0.16835954	0.13320697	0.1041358	0.19516181	11.53896461	11.53473488	11.51163415	11.53642189	11.49858231	11.48750535	11.46860448	11.56831524	11.46951114	11.60285996	11.56053715	11.5472621	11.51163415	11.35333728	11.36537534
NM_019827	Gsk3b	--	--	--	--	0.857189906	0.917417208	0.874287682	0.041931898	0.031215567	-0.00258941	0.012135553	0.14678535	10.08194985	10.06724024	9.988520194	10.07981837	10.0272999	10.03304116	10.0481661	10.06990867	10.01340809	10.22310225	10.13625458	10.18281592	10.03602057	10.00791245	10.04291419
NM_008927	Map2k1	--	--	--	--	0.707975641	0.859487444	0.928780391	0.786366271	0.06484592	0.05841333	0.01128136	0.0381458	10.90221148	10.95420631	10.98437426	10.87400416	10.95072213	10.94777372	10.88650378	10.90064175	10.92789463	10.92750619	10.94763697	10.92693714	10.97705799	10.88936039	10.88759514
NM_011952	Mapk3	down	--	--	--	0.008021259	0.012377608	0.024736711	0.448122734	-0.4409217	-0.27141057	-0.16186575	-0.03555903	10.75867544	10.7388364	10.68403822	10.95248658	10.87025653	10.908347	11.01789182	11.02585883	10.96409268	11.14619854	11.15866212	11.09137072	11.17975757	11.21192671	11.17006183
NM_008413	Jak2	--	--	--	--	0.18452948	0.113128249	0.085783974	0.124461246	0.363497588	0.315661558	0.329140933	0.279811678	7.389392089	7.577141169	7.689115479	7.529305139	7.77156398	7.495695582	7.473609452	7.710385966	7.542784514	7.493455259	7.417586559	7.621553086	7.568945327	7.0591505	7.213643581
NM_146145	Jak1	--	--	--	--	0.344951099	0.239696979	0.188233158	0.66079261	-0.113625033	-0.122180614	-0.109323749	0.0539118	9.922462231	9.923316127	9.997779761	9.902889512	9.998210354	9.914760546	9.927617411	9.965740174	9.895724335	10.1173677	10.07450217	10.09085296	10.14911841	9.985655615	10.03694116
NM_133872	Kdm1a	--	--	--	--	0.098244884	0.491351679	0.508656687	0.076034216	-0.13449044	-0.02954174	-0.0258367	0.11583082	11.29406189	11.28856278	11.324372	11.39901059	11.40973993	11.38290161	11.40271563	11.365013	11.41113083	11.54438315	11.51409714	11.54916463	11.42480865	11.42855233	11.47688573
NM_007971	Ezh2	--	--	--	--	0.954825324	0.520541013	0.952501056	0.988816343	0	-0.02035724	0.01417589	0.00739475	12.13368336	12.15222567	12.16144658	12.13186843	12.13728129	12.10926723	12.16940156	12.16890615	12.15523734	12.15962042	12.1711899	12.15222567	12.15222567	12.15227353	12.17995759
NM_001040400	Tet2	--	--	--	--	0.039743399	0.03808757	0.16460603	0.085863196	0.33152927	0.17416958	0.11812634	0.11460853	10.66612501	10.49800662	10.48743803	10.34124693	10.31256837	10.35798179	10.31856089	10.28520369	10.2116253	10.28168588	10.35434522	10.28041874	10.15633078	10.21274353	10.16707735
NM_007626	Cbx5	--	--	--	--	0.104771008	0.448512498	0.234366588	0.378675847	-0.1130471	-0.03324619	-0.0403085	0.04003962	11.9467603	11.98404002	11.96189243	12.04388512	11.99567834	12.04169334	12.03788678	12.03463103	12.02985775	12.08957936	12.1281104	12.11497915	12.07493953	12.05996135	12.08896336
NM_007622	Cbx1	--	--	--	--	0.029503499	0.031523059	0.09084253	0.242738549	-0.36432701	-0.22477881	-0.13733489	-0.0588725	10.50529175	10.56805632	10.66250848	10.70760452	10.72856585	10.61287766	10.75142734	10.79504844	10.86726985	10.87351075	10.83427461	10.88334215	10.93238333	10.92568575	11.00416614
NM_007624	Cbx3	--	--	--	--	0.125400264	0.212025786	0.050707961	0.578932935	0.14377367	0.082500588	0.175570951	0.059109856	9.369629651	9.26609133	9.268912178	9.224143305	9.15902597	9.207639096	9.315945681	9.300709459	9.207639096	9.184248364	9.088749562	9.193745451	9.10153102	9.125138508	9.137930853
NM_007872	Dnmt3a	down	down	down	down	5.79E-05	0.000156539	0.000394534	0.000423353	-2.614256669	-1.416622014	-0.89621702	-0.78195397	8.517299868	8.595657624	8.540243521	9.737878176	9.692769845	9.790956263	10.2811659	10.17247751	10.25828317	10.37254622	10.36961084	10.40209056	11.02348414	11.15450019	11.18834663
NM_001003961	Dnmt3b	down	down	down	down	8.89E-05	0.000407288	0.001073072	0.001584939	-2.38162021	-1.3013442	-0.67309286	-0.59547939	9.475157644	9.49111621	9.552179138	10.57139222	10.48226958	10.70994357	11.19964356	11.11466499	11.20354583	11.32857493	11.198151	11.27725703	11.78645283	11.87273642	11.9638793
NM_019448	Dnmt3l	down	down	--	--	7.20E-05	0.001784253	0.009081909	0.024567144	-2.140145475	-0.93206149	-0.32303863	-0.21060058	9.68469214	9.718660685	9.741563683	10.88282404	10.92674467	11.15320308	11.53576753	11.47950544	11.58499331	11.6861369	11.64820558	11.62409026	11.78159166	11.85889016	11.88153958
NM_027384	Tet1	down	down	down	--	0.012043531	0.001155823	0.003071994	0.188987465	-0.42177471	-0.52307951	-0.46890966	-0.0869057	11.83198186	11.78612132	11.73438113	11.68481652	11.64049752	11.68559214	11.85201809	11.73898637	11.7103168	12.16724092	12.12099033	12.09557375	12.21380166	12.17114233	12.20789603
NM_008709	Mycn	down	down	down	--	0.013255175	0.017733096	0.008417377	0.768439968	-0.6957288	-0.50192142	-0.51756819	-0.0490553	10.31278258	10.30103231	10.26090287	10.45473712	10.49483969	10.58456398	10.53634327	10.42601119	10.47919292	10.93964712	10.94770581	10.96206391	10.74352251	10.99955502	10.99676111
NM_010849	Myc	down	down	--	down	0.013617308	0.00289638	0.051284719	0.00095902	-0.889698966	-1.182810231	-0.414287531	-1.115077446	8.948131986	8.937675203	8.995396738	8.533296375	8.655020721	8.940751119	9.561489576	9.117559098	9.425543421	8.902701586	8.706861089	8.727253506	9.492794828	9.837630962	9.994381558
NM_183199	Usp44	down	down	down	down	0.000779259	0.000674732	0.003011611	0.000925336	-1.947622374	-1.108267546	-0.545201009	-0.696340342	6.994547718	7.16628917	7.424994803	8.005643998	8.054480223	7.882985553	8.568710535	8.486495177	8.598122343	8.417571202	8.409248914	8.456448046	9.113911544	9.075069593	9.290357453
BC150968	Pten	down	down	down	down	0.004347225	0.006175368	0.001199066	0.003978405	-0.935188344	-0.570273462	-0.528000839	-0.475490823	5.578639849	7.811929349	7.839265746	8.176844231	8.207157566	7.950639526	8.219116854	8.28933393	8.187012248	8.27096065	8.27162687	8.437611888	8.704290873	8.754209157	8.747117693
NM_011207	Ptpn3	down	down	down	down	0.004440574	0.001948325	0.00888838	0.001706495	-0.913158601	-0.804734379	-0.431924736	-0.604328065	8.325787749	8.435461897	8.365109234	8.473533456	8.528471108	8.428626633	8.718789125	8.904097049	8.846343099	8.67393977	8.67393977	8.660783444	9.276267835	9.216358731	9.456847074
NM_010203	Fgf5	down	down	down	down	0.003484177	0.001632991	0.003482057	0.00102103	-1.617623133	-1.493532399	-0.99527515	-1.257445917	7.11848357	7.127738512	7.103914189	7.475628506	7.204091533	7.242574304	7.843069138	7.566585779	7.740831553	7.471326069	7.478660786	7.56497826	8.337056459	8.736106703	9.140624536
NM_019479	Hes6	down	down	down	down	0.00186274	0.000984241	0.000628476	0.001928117	-1.02709816	-0.778450329	-0.683468263	-0.463202073	9.113122189	9.22012992	9.264193154	9.468777751	9.369580878	9.487614841	9.513085207	9.563759817	9.623797577	9.783694537	9.867355544	9.784026007	10.24722808	10.21997049	10.31767539
NM_023794	Etv5	down	down	down	down	0.00151885	0.000348124	0.00229291	0.000170104	-1.05308862	-1.28758063	-0.52562959	-0.72042855	10.25418848	10.3336498	10.19790214	9.989238588	10.01969647	10.2084079	10.88920744	10.73603722	10.78164751	10.58684855	10.60035282	10.57206562	11.37769272	11.3072771	11.29448691
NM_144763	Wt1	down	down	down	down	0.003550673	0.002019742	0.000958958	0.00038444	-1.440428912	-1.271910697	-1.246769169	-1.396640088	6.712424404	6.596103021	6.7446734	7.013497549	6.710421334	6.880760619	7.059348405	6.809774561	6.903902147	6.727946747	6.880760619	6.756031228	7.693281143	8.190188229	8.152671316
NM_175136	Rnf122	down	down	down	down	0.001033724	0.000640698	0.00047229	0.004211157	-1.406982756	-0.874992466	-0.800619676	-0.404030457	8.109772499	8.301907523	8.166331442	8.665307542	8.699863842	8.698321732	8.776723631	8.673796677	8.772694522	9.169283741	9.230628473	9.134220074	9.70048347	9.573314198	9.557400412
NM_020510	Frzd2	down	down	down	down	0.0011768	0.000624916	0.000618187	0.001556291	-1.477551854	-0.87747113	-0.737054155	-0.504505036	7.49228724	7.242459746	7.294703168	7.947765894	7.891149748	7.894783892	8.055733162	8.035200867	7.949156109	8.267749986	8.309992516	8.266084794	8.66412532	8.772255022	8.77786016

Supplemental table legend

Supplemental Table S1 (related to Figure 1E)

Quantitative gene expression data induced by combinatorial 2i treatments in ESCs

Bioinformatics data come from the GSE43597 in GEO DataSet.